

Keldysh pseudo-fermion functional renormalization group for quantum magnetism

Janik Potten,^{1,*} Yasir Iqbal,² Ronny Thomale,^{1,2} and Tobias Müller^{1,3}

¹*Institute for Theoretical Physics and Astrophysics, University of Würzburg, D-97074 Würzburg, Germany*

²*Department of Physics and Quantum Centre of Excellence for Diamond and Emergent Materials (QuCenDiEM), Indian Institute of Technology Madras, Chennai 600036, India*

³*Department of Physics, University of Zurich, Winterthurerstrasse 190, 8057 Zurich, Switzerland*

(Dated: March 17, 2025)

The functional renormalization group (FRG) approach for spin models relying on a pseudo-fermionic description has proven to be a powerful technique in simulating ground state properties of strongly frustrated magnetic lattices. A drawback of the FRG framework is that it is formulated in the imaginary-time Matsubara formalism and thus only able to access static correlations, a limitation shared with most other many-body approaches. A description of the dynamical properties of magnetic systems is the key to bridging the gap between theory and neutron scattering spectra. We take the decisive step of expanding the scope of pseudo-fermion FRG to the Keldysh formalism, which, while originally developed to address non-equilibrium phenomena, enables a direct calculation of the equilibrium dynamical spin structure factors on generic lattices in arbitrary dimension. We identify the principal features characterizing the low-energy spectra of exemplary zero-, one- and two-dimensional spin-1/2 Heisenberg models as well as the Kitaev honeycomb model.

I. INTRODUCTION

The field of frustrated magnetism is currently poised with the arrival of materials based on novel two- and three-dimensional lattice geometries promising to host a wealth of exotic quantum phases [1]. These span complex spin textures where the dipole moments form helices [2], skyrmions [3, 4], hedgehogs [5], vortex crystals or commensurate noncoplanar structures [6–8], as well as unconventional magnetic phases characterized by multipole order parameters [9, 10] such as quadrupolar (spin-nematic state) [11], octupolar [12], or even higher-rank orders [13, 14]. These phases feature nontrivial spin wave excitation spectra with characteristic fingerprints which allow for their identification based on inelastic neutron scattering profiles [15, 16]. The most intriguing scenario occurs when the system displays no magnetic order (either dipolar or multipolar) down to arbitrarily low temperatures, no sign of translation symmetry breaking, and no sharp magnon dispersion as it supports fractionalized spinon excitations, i.e., those quasiparticles formed in a *quantum spin liquid* state [17, 18]. Being generally defined by zero-temperature measurements, it is these very properties of QSLs rendering them notoriously difficult to describe theoretically, and to detect experimentally in comparison to other quantum fluids studied in condensed matter systems. Since, in most crystals, the strictly elastic limit is dominated by crystal defects and imperfections, one rather studies the data in the weakly inelastic domain above the disorder scale, which is still expected to share many features of the static signature in the idealized clean case. Thus, the most indicative, measurable quantity at hand is the dynamical spin structure factor obtained through inelastic neutron scattering.

Theoretically, there is neither a satisfactory microscopic description nor a fully adequate mean field theory available for QSLs. As much as major progress has been made within par-

ton approaches and spin liquid ground states, at the mean-field level, can now be adequately classified at the model level by structures such as their gauge group [19], there is still a disconnect between trial states generated from mean field theories and the microscopic Hamiltonian's ground state. From mean field theory, we further know that distinct types of spin liquids can look alike in terms of *static* correlations in finite size simulations yet might be significantly different in terms of their *dynamic* correlation profile. The problem here is that one can only generate static, but not dynamic, spin correlators from ground state wave functions. While recent attempts [20, 21] have been made at computing dynamical spin structure factors beyond mean-field, they are limited in scope by the class of excitations of the matter fields that can be constructed while gauge-field excitations, which are known to be crucial for QSLs, are not *a priori* accounted for. The current effort of the theory community in frustrated magnetism thus focuses on finding ways to access dynamical spin correlations in higher dimensional quantum paramagnets. In doing so, in addition to acquiring a better identification tool for spin liquids states, one also attempts to address the fundamental question of how $S = 1$ magnon excitations in an ordered magnet dissociate into fractional $S = 1/2$ spinon excitation as one approaches the paramagnetic regime across a quantum critical point. A convincing theoretical analysis has so far only been accomplished in spin chains [22]. In two spatial dimensions, where analytically exact limits are less available than for spin chains, progress has been recently reported from density matrix renormalization group (DMRG) studies [23, 24]. Similarly, variational Monte Carlo methods can in principle be generalized to track energy expectation values of excited trial states. In both cases, however, frustrated magnets in 3D, which is the regime where current new material candidates for spin liquids are predominantly identified [25–27], pose a nearly unsurmountable challenge either due to entanglement growth (DMRG) or due to increases in the number of wave function parameters (Monte Carlo).

In order to calculate dynamical spin correlations for 2D and, in particular, 3D quantum paramagnets, here we develop

* Corresponding author: janik.potten@uni-wuerzburg.de

a Keldysh formulation of the pseudofermion functional renormalization group (PFFRG) [28]. Our starting point is the Matsubara formulation of the PFFRG [29], as it was refined and optimized in recent years. While the Keldysh form is suited to calculate non-equilibrium phenomena as well [30–36], our predominant motivation lies in avoiding analytic continuation from the imaginary to the real frequency axis as we attempt to access the dynamical response functions, which has so far been inaccessible within the PFFRG (except for particular cases in which a Padé approximation was applicable [37]).

This paper is organized as follows. After a short introduction of Abrikosov pseudo-fermions (Section II) and the main building blocks of the Keldysh formalism (Section III), we formulate the Keldysh pseudo-fermion functional renormalization group in Section IV. There, we also detail its classical large- S limit (Section IV A), as well as performing detailed symmetry analysis of the relevant vertex functions (Section IV B), the definition of relevant observables (Section IV C) and the numerical implementation (Section IV D). We benchmark the method in Section V for the zero-dimensional Heisenberg dimer (Section V A), the one-dimensional spin chain (Section V B), as well as the two-dimensional Square lattice (Section V C) and Kitaev-Honeycomb (Section V D) models. Finally, we conclude in Section VI that our Keldysh implementation of the pseudofermion FRG promises to be a key advancement in rendering the dynamical fingerprint of a frustrated magnet accessible within the scope of functional renormalization group.

II. ABRIKOSOV PSEUDO FERMIONS

In this paper we will consider a family of possibly anisotropic spin Hamiltonians

$$H = \sum_{\substack{i,j \\ \mu,\nu}} J_{ij}^{\mu\nu} S_i^\mu S_j^\nu \quad (1)$$

which includes e.g., the Heisenberg model with $J_{ij}^{\mu\nu} \equiv J_{ij} \delta_{\mu\nu}$ and the Kitaev model. It can be derived as a strong coupling limit from the Hubbard model at half-filling and is well suited to describe localized interacting electron spins. However, due to the canonical commutation relations of the spin operators, which are neither fermionic nor bosonic, and the resulting inapplicability of Wick's theorem, standard many-body techniques are not straightforwardly applicable to (1) [28]. Especially, a rigorous formulation of the flow equations using the spin operators proves to be cumbersome [38] and they have so far only been solved in limiting cases [39–45], while a numerical implementation is still at large.

One way of circumventing this obstacle is to introduce an auxiliary fermion representation [46] of the spin operators

$$S_i^\mu = \sum_{\beta,\beta'} \frac{1}{2} f_{i\beta}^\dagger \sigma_{\beta\beta'}^\mu f_{i\beta'}. \quad (2)$$

With this reformulation, the Hamiltonian takes the form

$$H_{\text{PF}} = \sum_{\substack{i,j \\ \mu,\nu}} \sum_{\beta_1,\beta'_1} \sum_{\beta_2,\beta'_2} \frac{J_{ij}^{\mu\nu}}{4} \sigma_{\beta_1\beta'_1}^\mu \sigma_{\beta_2\beta'_2}^\nu f_{i\beta_1}^\dagger f_{j\beta_2}^\dagger f_{j\beta'_2} f_{i\beta'_1} \quad (3)$$

To render the mapping in (2) exact, one has to introduce the constraint

$$\sum_{\beta} f_{i\beta}^\dagger f_{i\beta} = 1 \quad (4)$$

on the particle number since the fermion decomposition doubles the Hilbert space and allows also for empty or doubly-occupied sites, which do not map to a physical spin state. For this reason, these fermions are often referred to as pseudo-fermions. There is a technique originally proposed by V. Popov and S. Fedotov [47, 48] to fulfill this constraint exactly using an imaginary chemical potential but its treatment is out of the scope of this paper [see [49, 50]]. Further, there is also a pseudo-Majorana approach for the Heisenberg model [51, 52], which is able to circumvent this constraint with the decomposed Hilbert space only being physical. This will be a future path for our technique and is also not further discussed here.

In the following we will assume that the constraint is not fulfilled exactly but rather on average. This will be investigated in detail for the anti-ferromagnetic (AFM) dimer in Sec. V A.

III. KELDYSH FORMALISM

The Keldysh formalism was originally proposed as a framework to describe non-equilibrium phenomena [53]. Here, we employ it to introduce real frequencies into our formalism, diverging from the conventional use of imaginary Matsubara frequencies, while still maintaining equilibrium conditions. We will only provide a brief overview of the main ideas and refer to the literature [30] for a detailed introduction.

Non-equilibrium dynamics potentially evolves the ground state beyond acquiring a dynamical phase. Adding another dimension of complexity to the calculation of expectation values. To illustrate, we consider a generic, time-dependent Hamiltonian $H(t)$. The system is then described by the time-evolution operator

$$U_{t,t'} = \text{T exp} \left(-i \int_{t'}^t H(\tau) d\tau \right), \quad (5)$$

where T denotes time ordering. Assuming the system is initially in the state described by the density matrix $\rho(-\infty)$, at time t , it is given by

$$\rho(t) = U_{t,-\infty} \rho(-\infty) U_{t,-\infty}^\dagger. \quad (6)$$

Using this, the expectation value of an observable \mathcal{O} at a given

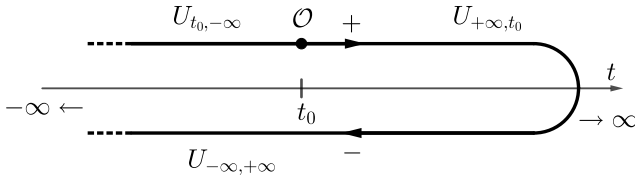


Figure 1. Keldysh contour with an operator \mathcal{O} inserted at $t = t_0$. The respective time propagation operators are also given.

time t_0 can be expressed as:

$$\begin{aligned} \langle \mathcal{O}(t_0) \rangle &= \text{tr}[\mathcal{O}\rho(t_0)] / \text{tr}[\rho(t_0)] \\ &= \text{tr}[U_{-\infty, t_0} \mathcal{O} U_{t_0, -\infty} \rho(-\infty)] / \text{tr}[\rho(t_0)] \\ &= \text{tr}[U_{-\infty, \infty} U_{\infty, t_0} \mathcal{O} U_{t_0, -\infty} \rho(-\infty)] / \text{tr}[\rho(-\infty)] \end{aligned} \quad (7)$$

In the last step we introduced $U_{t_0, \infty} U_{\infty, t_0}$ as a representation of unity which formally closes the time contour of the Keldysh formalism at $t = -\infty$. This time contour, depicted in Fig. 1, consists of two branches, which are the forward-propagating (denoted by +) and backward-propagating (-) one.

When calculating expectation values the operators thus have to be contour ordered (denoted by \mathcal{C}), as placing an operator on the forward propagating branch can have a different effect than on the backward propagating branch. This also necessitates four different Green's functions

$$\begin{pmatrix} G^{++} & G^{+-} \\ G^{-+} & G^{--} \end{pmatrix} \equiv \begin{pmatrix} G^T & G^< \\ G^> & G^{\tilde{T}} \end{pmatrix} \quad (8)$$

which are given by $iG^{\eta\eta'} = \langle \mathcal{C} f^\eta f^{\eta'} \rangle$ with $\eta^{(\prime)} = \pm$. The latter notation consisting of time ordered (G^T), anti-time ordered ($G^{\tilde{T}}$), lesser ($G^<$) and greater ($G^>$) Green's functions is typically found in the literature.

The formal closure of the contour introduces an ambiguity in the formalism, as at this point no contour index can be assigned. This leads to a redundancy in the Green's function, which can be removed by performing the basis transformation

$$A = \frac{1}{\sqrt{2}} \begin{pmatrix} 1 & -1 \\ 1 & 1 \end{pmatrix} \quad (9)$$

which results in

$$A \begin{pmatrix} G^{++} & G^{+-} \\ G^{-+} & G^{--} \end{pmatrix} A^{-1} = \begin{pmatrix} 0 & G^{\text{av}} \\ G^{\text{ret}} & G^{\text{K}} \end{pmatrix}, \quad (10)$$

where G^{ret} and G^{av} are the typical advanced and retarded Green's functions and G^{K} is an additional Keldysh Green's function. In equilibrium, the latter is fully determined by the fluctuation dissipation theorem

$$G^{\text{K}}(\omega) = (1 - 2n_{\text{F}}(\omega))(G^{\text{ret}}(\omega) - G^{\text{av}}(\omega)). \quad (11)$$

The independent Green's functions for a free-fermion with

$H_0 = \epsilon_0 f^\dagger f$ in Fourier space are given by

$$G_0^{\text{ret/av}}(\omega) = \lim_{\eta \rightarrow 0} \frac{1}{\omega - \epsilon_0 \pm i\eta}. \quad (12)$$

For both formulae we used the Fourier transformation given by

$$G(\omega) = \int e^{i\omega t} G(t) dt, \quad (13)$$

$$G(t) = \frac{1}{2\pi} \int e^{-i\omega t} G(\omega) d\omega. \quad (14)$$

IV. PSEUDO-FERMION FUNCTIONAL RENORMALIZATION GROUP

In this section, we will bring the concepts of auxiliary fermions and the Keldysh formalism together with the functional renormalization group (FRG). The general framework of RG is based on Wilson's idea for quantum many-particle systems [54] which formulates an effective low energy theory by integrating out all high energy degrees of freedom. This is done by artificially introducing a cutoff parameter Λ into our theory $G_0 \rightarrow G_0^\Lambda$ which fulfills the properties

$$G_0^{\Lambda=\infty} = 0, \quad G_0^{\Lambda=0} = G_0. \quad (15)$$

This is not necessarily the only starting condition for $\Lambda = \infty$ in the FRG formalism since there exist other e.g. from a correlated initial state for the fermionic Hubbard-model [55]. However, shutting off all particle dynamics is very practical in our case, arriving at the conditions above. Since, our Hamiltonian is quartic in terms of the pseudo-fermions we have a free theory with no kinetic (quadratic) term. We can thus use the free particle Green's functions Eq. (12) with $\epsilon_0 = 0$. For the cutoff, there are in principle different choices [56], as the conditions Eq. (15) are relatively weak but it has been shown that a cutoff using the convergence parameter for advanced and retarded Green's functions preserves the most symmetries of the system – especially causality – and thus should be used [57, 58]. The bare propagators thus read

$$G_0^{\Lambda \text{ ret/av}}(\omega) = \frac{1}{\omega \pm i\Lambda} \quad (16)$$

while the Keldysh component is still given via the fluctuation-dissipation theorem Eq. (11). Employing this cutoff we can formulate differential equations which allow us to calculate the low energy properties of the system by successively integrating in degrees of freedom. For the FRG we formulate these flow equations directly in terms of the one-particle irreducible vertex functions.

Compared to the more standard Matsubara formulation [28], the derivation of the Keldysh flow equations only deviates at two points. Firstly, there is an imaginary unit present in the time evolution operator Eq. (5) and secondly the definitions of the Green's functions likewise feature another imaginary i . These exactly cancel each other [59, 60],

leaving the actual flow equations form-invariant between the two formulations. For the one- and two-particle vertex functions γ_1 and γ_2 these are given by

$$\frac{d}{d\Lambda} \gamma_1^\Lambda(1'|1) = \sum_{22'} \gamma_2^\Lambda(1', 2'|1, 2) S^\Lambda(2|2') \quad (17)$$

and

$$\begin{aligned} \frac{d}{d\Lambda} \gamma_2^\Lambda(1', 2'|1, 2) &= \sum_{33'} \gamma_3^\Lambda(1', 2', 3'|1, 2, 3) S_{33'}^\Lambda \\ &+ \sum_{33'} \sum_{44'} [\gamma_2^\Lambda(1', 2'|3, 4) \gamma_2^\Lambda(3', 4'|1, 2) \\ &- \gamma_2^\Lambda(1', 4'|1, 3) \gamma_2^\Lambda(3', 2'|4, 2) - (3^{(\prime)} \leftrightarrow 4^{(\prime)}) \\ &+ \gamma_2^\Lambda(2', 4'|1, 3) \gamma_2^\Lambda(3', 1'|4, 2) + (3^{(\prime)} \leftrightarrow 4^{(\prime)})] G_{33'}^\Lambda S_{44'}^\Lambda \end{aligned} \quad (18)$$

Here, we have used multi-indices k which consist of all relevant quantum numbers for the problem at hand. S denotes the so-called single-scale propagator

$$S^\Lambda = G^\Lambda [\partial_\Lambda (G_0^\Lambda)^{-1}] G^\Lambda. \quad (19)$$

As illustrated in Eq. (18), the n -particle vertex always couples to the $n+1$ -particle vertex in the flow. Therefore, to arrive at a closed set of differential equations, this hierarchical structure has to be broken, which we do by neglecting all $n > 2$ -particle contributions, setting $\gamma_{n>2} = 0$. As usual for the PFFRG this is remedied partially by using the Katanin substitution

$$S^\Lambda \rightarrow \frac{d}{d\Lambda} G^\Lambda, \quad (20)$$

which was shown to fulfill the Ward identities up to one order higher [61] for certain diagrams. The effect of the truncation will be discussed in the following sections.

Further, using the tree expansion one can relate the single particle vertex function to the self-energy Σ by $\gamma_1 \equiv -\Sigma$ [62]. This allows for the calculation of the full Green's function by Dyson's equation

$$G_{\text{Full}} = (G_0^{-1} - \Sigma)^{-1} \quad (21)$$

Thus, we will use $\Sigma \equiv -\gamma_1$ in the following and also rename the two particle vertex function as $\Gamma \equiv \gamma_2$ for consistency with previous literature.

For the pseudo-fermion FRG the relevant parameters consist of $k = \{\omega_k, i_k, \beta_k, \alpha_k\}$ where ω is the frequency, i is the lattice site, β is the spin index and α is the Keldysh index. We assume that all one-particle quantities such as the self-energy Σ and the Green's function G only act locally, are diagonal in spin space and fulfill energy conservation. Using this we get

$$\Sigma(1'|1) = \Sigma^{\alpha'_1 \alpha_1}(\omega_1) \delta(\omega_1 - \omega'_1) \delta_{i'_1 i_1} \delta_{\beta'_1 \beta_1} \quad (22)$$

The condition of locality is a consequence of the decomposi-

tion into pseudo fermions. This will be discussed in detail in Sec. IV B. For the two-particle functions one similarly gets a bi-locality condition. This allows for the vertex to be decomposed as

$$\begin{aligned} \Gamma(1', 2'|1, 2) &= \\ &\{ [\Gamma_{\mu\nu i_1 i_2}^{\alpha'_1 \alpha'_2 \alpha_1 \alpha_2}(\omega'_1 \omega'_2 | \omega_1 \omega_2) \sigma_{\beta'_1 \beta_1}^\mu \sigma_{\beta'_2 \beta_2}^\nu \\ &+ \Gamma_{d i_1 i_2}^{\alpha'_1 \alpha'_2 \alpha_1 \alpha_2}(\omega'_1 \omega'_2 | \omega_1 \omega_2) \delta_{\beta'_1 \beta_1} \delta_{\beta'_2 \beta_2}] \delta_{i'_1 i_1} \delta_{i'_2 i_2} \\ &- [\Gamma_{\mu\nu i_2 i_1}^{\alpha'_1 \alpha'_2 \alpha_2 \alpha_1}(\omega'_1 \omega'_2 | \omega_2 \omega_1) \sigma_{\beta'_1 \beta_2}^\mu \sigma_{\beta'_2 \beta_1}^\nu \\ &+ \Gamma_{d i_2 i_1}^{\alpha'_1 \alpha'_2 \alpha_2 \alpha_1}(\omega'_1 \omega'_2 | \omega_2 \omega_1) \delta_{\beta'_1 \beta_2} \delta_{\beta'_2 \beta_1}] \delta_{i'_1 i_2} \delta_{i'_2 i_1} \} \\ &\times \delta(\omega_1 + \omega_2 - \omega_{1'} - \omega_{2'}). \end{aligned} \quad (23)$$

Here, we used the fermionic properties under particle permutation and performed a basis decomposition in terms of spin components $\Gamma_{\mu\nu}$ and a density component Γ_d using the Pauli matrices (σ^μ with $\mu \in x, y, z$) and the unit matrix ($\sigma^{\mu=0} \equiv \mathbb{1}$). For an isotropic (Heisenberg) spin interaction one can assume $\Gamma_{\mu\nu} = \Gamma_s \delta_{\mu\nu}$, $\forall \mu, \nu$ which further simplifies the decomposition. The anisotropic Heisenberg model with $\Gamma_{\mu\nu} = \Gamma_\mu \delta_{\mu\nu}$ also includes the XXZ model or the Kitaev-Heisenberg model. The full flow equations for the anisotropic vertices can be found in Appendix A.

The initial conditions in the Keldysh basis are given by

$$\Gamma_{\mu\nu i_1 i_2}^{\alpha'_1 \alpha'_2 \alpha_1 \alpha_2, \Lambda \rightarrow \infty} = -i \frac{J_{ij}^{\mu\nu}}{4} \bar{v}^{\alpha'_1 \alpha'_2 \alpha_1 \alpha_2} \quad (24)$$

where only the spin vertices are initialized and the Keldysh structure is given by [31]

$$\bar{v}^{1'2'12} = \begin{cases} \frac{1}{2} & (1' = 1 \wedge 2' \neq 2) \vee (1' \neq 1 \wedge 2' = 2) \\ 0 & \text{otherwise.} \end{cases} \quad (25)$$

A. Large- S Limit

There are different limits in which the FRG equations simplify into a system which is easier to solve [63, 64]. One of these is the large S limit, where the spin length of the localized moments goes to infinity. This renders the system classical in the sense, that the spins act like classical vectors, as the commutators scale with $1/S$ and thus vanish for $S \rightarrow \infty$ [65, 66]. In this limit only the second line in Eq. (18) is non-zero, which – diagrammatically written – is a typical RPA-like ladder and can be solved directly by utilizing the geometric series. This is possible since the self-energy flow vanishes in this limit.

Formally, the full two-particle vertex in this limit can be written as

$$\Gamma_{\text{RPA}} = \Gamma_{\text{bare}} + \Gamma_t. \quad (26)$$

Using the now exact Bethe-Salpeter equation

$$\Gamma_t = \frac{1}{\pi} \oint d\Omega G \Gamma_{\text{bare}} \Gamma_{\text{RPA}} G, \quad (27)$$

where we denote all internal summations and integrations by $\oint d\Omega$ for brevity. This leads to the infinite ladder, when inserting into Eq. (26). The solution is given by

$$\Gamma_{i_1 i_2, \text{RPA}}^{1' 2' 1 2} (t) = \sum_j \sum_{3 4'} \Gamma_{i_1 j, \text{bare}}^{1' 4' 1 3} R_{j i_2}^{3 2' | 4' 2} (t) \quad (28)$$

where R is calculated via

$$R \equiv \left(\mathbf{1}_{j i_2}^{3 2' 4' 2} - \frac{1}{\pi} \sum_{3' 4'} \Gamma_{j i_2, \text{bare}}^{3' 2' 4 2} \int d\nu G_{3 3'}^\Lambda (t + \nu) G_{4 4'}^\Lambda (\nu) \right)^{-1} \quad (29)$$

which is the result of the geometric series. The inversion can be performed using standard matrix inversion for m_{ij} by rearranging the indices so that all summation indices ($j, 3, 4'$) are found in i and the outside indices are in j . This assures, that m^k is well-defined by standard matrix multiplication and thus also $R = m^{-1}$. Thus, we can calculate the irreducible vertex Γ for the physical system with $\Lambda = 0$, as the formulation of the RPA does not need an energy cutoff. However, this results in integrals with peaked integrands, which is why we introduce a finite Λ to evaluate the RPA. Further, introducing the cutoff into the RPA allows us to compare the FRG results with the exact RPA results, to check whether the numerical implementation performs at the desired accuracy. This will be discussed in Sec. V A 1.

B. Symmetry Analysis

An efficient numerical implementation of Keldysh PFFRG will necessitate the implementation of all possible symmetries of the system which are either due to the chosen model or general symmetries of the formalism. We will here bring together the general symmetries in the PFFRG [28] with the specific formulations for the Keldysh formalism, as laid out by Jakobs [58].

1. General Symmetries

We start by the general symmetries of the formalism. For this we define a general n -particle Green's function as

$$i^n G_{q|q'}^{\eta|\eta'}(\mathbf{t}|\mathbf{t}') = \langle \mathcal{C} f_{q_1}^{\eta_1}(t_1) \dots f_{q_n}^{\eta_n}(t_n) f_{q'_n}^{\eta'_n \dagger}(t'_n) \dots f_{q'_1}^{\eta'_1 \dagger}(t'_1) \rangle \quad (30)$$

where the bold variables denote all of the n corresponding variables and q represents all necessary quantum numbers except the Keldysh indices and the time/frequency (i.e., the lattice site or the spin index). The Keldysh indices are denoted as $\eta = \pm$ in the contour and as $\alpha = 1, 2$ in the Keldysh basis,

respectively. For better readability we separate the indices of incoming and outgoing particles explicitly (e.g., $\eta|\eta'$). For the Fourier transformation into frequency space we use the convention from Eqs. (13) and (14).

The first symmetry we consider already featured in Sec. III, where we introduced the Keldysh rotation. If one time argument is strictly greater than all others, the contour index for this particle is ill-defined as the contour was artificially extended to $t \rightarrow \infty$ from the largest time. This is exploited by the Keldysh rotation. Applying the Keldysh rotation only to the contour index with the largest time yields

$$G_{q|q'}^{1, \eta_2 \dots \eta_n | \eta'}(\mathbf{t}|\mathbf{t}') = 0 \quad \text{if } t_1 > t_2 \dots t_n. \quad (31)$$

This means that in frequency space the Green's function with all Keldysh indices $\alpha_i = 1$ fulfills

$$G_{q|q'}^{1 \dots 1 | 1 \dots 1}(\omega|\omega') = 0 \quad (32)$$

For the vertex functions there exists a similar relation [57]

$$\gamma_{q|q'}^{2 \dots 2 | 2 \dots 2}(\omega|\omega') = 0. \quad (33)$$

This can be easily understood by Dyson's equation Eq. (21) and the relation between the vertex and Green's functions.

Next, we turn to the transformation of Green's functions under complex conjugation, which can directly be inferred from Eq. (30) as

$$G_{q|q'}^{\eta|\eta'}(\mathbf{t}|\mathbf{t}')^* = (-1)^n G_{q'|q}^{\bar{\eta}|\bar{\eta}}(\mathbf{t}'|\mathbf{t}) \quad (34)$$

where the bar denotes a switch in the contour from one branch to the other ($\pm \rightarrow \mp$). The pre-factor is due to the imaginary units in the definition of the Green's function. We do not get additional minus signs from contour ordering the operators, since they always come in pairs. For the Keldysh basis in frequency space the same relation is given by

$$G_{q|q'}^{\alpha|\alpha'}(\omega|\omega')^* = (-1)^{n + \sum_k (\alpha_k + \alpha_{k'})} G_{q'|q}^{\alpha'|\alpha}(\omega'|\omega) \quad (35)$$

where the exchange of the branch now only results in an additional pre-factor and leaves the indices unchanged. Since the vertex functions are closely related to the Green's functions due to the tree expansion and Dyson's equation, all of the remaining symmetries are also applicable to the vertex functions while sometimes the pre-factors are slightly different [57, 64]. We will thus only use the Green's functions in the following.

The third symmetry is invariance under global time translations, which originates in the time-independence of the equilibrium Hamiltonian Eq. (3). This allows us to always perform a global time translation of our operators resulting in an energy conservation relation in frequency space

$$G_{q|q'}^{\eta|\eta'}(\omega|\omega') = G_{q|q'}^{\eta|\eta'}(\omega|\omega') \delta \left(\sum_{k=1}^n (\omega'_k - \omega_k) \right). \quad (36)$$

Further, we have the crossing symmetry. Due to the

$\Gamma^{2222}(1'2' 12) = 0$	(CS)
$\Gamma^{\alpha'_1\alpha'_2 \alpha_1\alpha_2}(1'2' 12) = (-1)^{\sum_k(\alpha_k+\alpha'_k)}\Gamma^{\alpha_1\alpha_2 \alpha'_1\alpha'_2}(12 1'2')^*$	(CC)
$\Gamma^{\alpha'_1\alpha'_2 \alpha_1\alpha_2}(1'2' 12) = \Gamma^{\alpha'_1\alpha'_2 \alpha_1\alpha_2}(1'2' 12)\delta(\omega'_1 + \omega'_2 - \omega_1 - \omega_2)$	(TT)
$\Gamma^{\alpha'_1\alpha'_2 \alpha_1\alpha_2}(1'2' 12) = \Gamma^{\alpha'_1\alpha'_2 \alpha_1\alpha_2}(1'2' 12)\delta_{i_1i'_1}\delta_{i_2i'_2} - \Gamma^{\alpha'_1\alpha'_2 \alpha_2\alpha_1}(1'2' 21)\delta_{i_2i'_1}\delta_{i_1i'_2}$	(U(1))
$\Gamma^{\alpha'_1\alpha'_2 \alpha_1\alpha_2}(1'2' 12)\delta_{i_1i'_1}\delta_{i_2i'_2} = -\Gamma^{\alpha'_1\alpha'_2 \alpha_2\alpha_1}(1'2' 21)\delta_{i_2i'_1}\delta_{i_1i'_2} = -\Gamma^{\alpha'_2\alpha'_1 \alpha_1\alpha_2}(2'1' 12)\delta_{i_1i'_2}\delta_{i_2i'_1}$	(X)
$\Gamma^{\alpha'_1\alpha'_2 \alpha_1\alpha_2}(1'2' 12)\delta_{i_1i'_1}\delta_{i_2i'_2} = -\beta'_1\beta_1\Gamma^{\alpha_1\alpha'_2 \alpha'_1\alpha_2}(-12' 1'2)\delta_{i_1i'_1}\delta_{i_2i'_2}$	(PH1)
$\Gamma^{\alpha'_1\alpha'_2 \alpha_1\alpha_2}(1'2' 12)\delta_{i_1i'_1}\delta_{i_2i'_2} = -\beta'_2\beta_2\Gamma^{\alpha'_1\alpha_2 \alpha_1\alpha'_2}(1'-2 1-2')\delta_{i_1i'_1}\delta_{i_2i'_2}$	(PH2)

Table I. All symmetries of the two particle vertex function used in this work. We explicitly write out the Keldysh indices for all symmetries even if they remain unchanged. (CS) is the causality relation, (CC) is the symmetry under complex conjugation in the Keldysh basis, (TT) is the symmetry under global time translations, (U(1)) is the U(1) gauge freedom, (X) is the crossing symmetry and (PH1) and (PH2) denote the particle-hole conjugation in the first or second particle. The pre-factor for the (CC) symmetry misses a -1 compared to reference [58] since the vertex definition contains an additional imaginary unit.

fermionic nature of the operators we get

$$\begin{aligned} G_{q|P(q')}^{\alpha|P(\alpha')}(\omega|P(\omega')) &= G_{P(q)|q'}^{P(\alpha)|\alpha'}(P(\omega)|\omega') \\ &= (-1)^P G_{q|q'}^{\alpha|\alpha'}(\omega|\omega') \end{aligned} \quad (37)$$

where P denotes an arbitrary permutation and $(-1)^P$ is the resulting sign due to the total number of fermionic permutations.

We can also make use of all symmetries, that map equivalent lattice points onto another. We will denote those symmetry operations by $L(i)$. This leaves all other quantum numbers unchanged. We get

$$G_{i|i'}(1|1') = G_{L(i)|L(i')}(1|1') \quad (38)$$

and similarly for the two particle Green's functions and the vertex functions.

Note that we will not use the symmetry under time reversal. This is due to the contour ordering of the operators, which would also be reversed under this operation, leading to anti-contour ordered Green's functions. In equilibrium one can use this to extract generalized fluctuation-dissipation theorems [57], which we will not use due to their complicated Keldysh structure, thus rendering a numerical implementation unfeasible [67]. However, they can be applied as a check of the symmetry violation of the implementation.

2. PFFRG Specific Symmetries

The two specific symmetries result from the invariance under local SU(2) rotations of the pseudo-fermion decomposition Eq. (2) and thus the Hamiltonian Eq. (3). Since, a general SU(2) transformation would give a linear combination of creation and annihilation operators, the evaluation of the resulting expectation values would give a mixture of different operators. Due to this, we only choose the subgroups that have a one-to-one mapping in the operators. Those are the U(1) and the \mathbb{Z}_2 .

The transformation of the pseudo-fermion operators under

local U(1) operations can be written as

$$g_{\varphi_i} \begin{pmatrix} f_{i\beta'}^{\eta\dagger} \\ f_{i\beta}^{\eta} \end{pmatrix} g_{\varphi_i}^{-1} = \begin{pmatrix} e^{i\varphi_i} f_{i\beta'}^{\eta\dagger} \\ e^{-i\varphi_i} f_{i\beta}^{\eta} \end{pmatrix} \quad (39)$$

which is just the multiplication by a phase φ_i at lattice site i . For the one-particle Green's function, invariance under this transformation leads to the condition

$$G_{i|i'}(1|1') \stackrel{!}{=} e^{i(\phi_{i'} - \phi_i)} G_{i|i'}(1|1') \quad (40)$$

Since, the phase is independent on all lattice sites, this fixes the one particle functions to be local and, likewise, all two particle functions to be bi-local. The \mathbb{Z}_2 operations are the particle-hole conjugations

$$g_{\text{PH}} \begin{pmatrix} f_{i\beta}^{\eta\dagger} \\ f_{i\beta}^{\eta} \end{pmatrix} g_{\text{PH}}^{-1} = \begin{pmatrix} \beta f_{i\bar{\beta}}^{\eta} \\ \beta f_{i\bar{\beta}}^{\eta\dagger} \end{pmatrix} \quad (41)$$

where $\bar{\beta}$ denotes a flipped spin index. Note, that this symmetry always has to be applied to both branches, thus allowing for the symmetry to be used for arbitrary Keldysh indices.

For the one-particle Green's function this results in

$$G_{\beta|\beta'}^{\alpha|\alpha'}(\omega|\omega')\delta_{ii'} = -\beta\beta' G_{\bar{\beta}|\bar{\beta}'}^{\alpha|\alpha'}(-\omega'|\omega)\delta_{ii'}. \quad (42)$$

and can be cross checked easily for the free particle propagators. For the two-particle Green's function we get

$$\begin{aligned} G_{\beta_1\beta_2|\beta'_1\beta'_2}^{\alpha_1\alpha_2|\alpha'_1\alpha'_2}(\omega_1\omega_2|\omega'_1\omega'_2)\delta_{i_1i'_1}\delta_{i_2i'_2} \\ = -\beta_1\beta'_1 G_{\bar{\beta}'_1\bar{\beta}'_2|\bar{\beta}_1\bar{\beta}_2}^{\alpha'_1\alpha'_2|\alpha_1\alpha_2}(-\omega'_1\omega_2|\omega_1\omega_2)\delta_{i_1i'_1}\delta_{i_2i'_2} \\ = -\beta_2\beta'_2 G_{\bar{\beta}_1\bar{\beta}_2|\bar{\beta}'_1\bar{\beta}'_2}^{\alpha_1\alpha_2|\alpha'_1\alpha'_2}(\omega_1-\omega_2|\omega'_1-\omega_2)\delta_{i_1i'_1}\delta_{i_2i'_2} \end{aligned} \quad (43)$$

where both corresponding particle-hole pairs can be mapped independently.

A list of all vertex symmetries used in this paper is presented in Table I. The combinations of symmetries used in the numerical implementation are given in Appendix D for com-

pleteness.

C. Observables

The PFFRG equations inherently respect all symmetries present in the initial conditions, i.e. the model as defined by the Hamiltonian. Therefore, no order parameters, such as a magnetization in the case of magnetic order, can become finite during the flow. To enter the symmetry broken phase during the RG procedure, one would have to include an small initial ordering tendency, which could be realized, e.g., through an infinitesimal magnetic field to probe for magnetic orders. If this initial order is accepted by the system, the corresponding magnetization then will become finite during the flow [68, 69]. This procedure, however, requires an *a priori* guess for the ordering tendency, which introduces a bias in the method. Therefore we refrain from this technique and defer it to future research.

Instead, we use the magnetic susceptibility and the corresponding spin structure factor as a measure for ordering tendencies. If the system wants to order during the flow from the initially paramagnetic phase, this is signaled by a divergence of the magnetic susceptibility and breakdown of the RG flow. A lack of such a divergence signals a magnetically disordered ground state and therefore a possible spin liquid candidate phase.

To find an expression for the susceptibility in terms of pseudo fermions, we start by assuming that the action \mathcal{S} in principle has two source terms for the spin along the z direction

$$\mathcal{S} \propto h_+ S^{z,+} - h_- S^{z,-} \quad (44)$$

since we can either put an operator on the $+$ or on the $-$ branch. The magnetic susceptibility in the contour basis then can be calculated using $\chi^{\pm\pm} = \partial \log(Z) / \partial h_{\pm} \partial h_{\pm} |_{h_{\pm} \rightarrow 0}$ where Z

is the partition function. To get a physical result however, one has to calculate the retarded susceptibility, which can be done by either rotating the result of the susceptibility calculations afterwards, or by rotating directly in the action. We will choose the latter variant.

After the decomposition using Eq. (2) and rotation with $f^1 = 1/\sqrt{2}(f^+ - f^-)$ and $f^2 = 1/\sqrt{2}(f^+ + f^-)$ (cf. Eq. (9)) we get

$$\begin{aligned} \mathcal{S}_{\text{mag}} &\propto \sum_{\alpha\alpha'\beta\beta'} h_1 (f_{\alpha'}^{1\dagger} \sigma_{\alpha'\alpha}^z f_{\alpha}^1 + f_{\alpha'}^{2\dagger} \sigma_{\alpha'\alpha}^z f_{\alpha}^2) \\ &\quad + h_2 (f_{\beta'}^{1\dagger} \sigma_{\beta'\beta}^z f_{\beta}^1 + f_{\beta'}^{2\dagger} \sigma_{\beta'\beta}^z f_{\beta}^2) \quad (45) \\ &\equiv \sum_{\alpha\alpha'\beta\beta'} V_q \rho_{cl} + V_{cl} \rho_q. \end{aligned}$$

Here, the last line represents the standard naming for an arbitrary field with sources V [30] with $V_q \equiv h_1$ and $V_{cl} \equiv h_2$. The real space spin susceptibility can then be calculated by

$$\begin{aligned} \chi_{ij}^{\text{Ret}} &= \langle S_i^z S_j^z \rangle_{\text{ret}} = \frac{\delta \rho_{cl}}{\delta V_{cl}} = \frac{1}{2i} \frac{\delta^2 \log(Z)}{\delta V_{cl} \delta V_q} \quad (46) \\ &= \frac{i}{2} \sum_{\alpha\alpha'\beta\beta'} \sigma_{\alpha'\alpha}^z \sigma_{\beta'\beta}^z (G_{\text{Full}}^{12|11} + G_{\text{Full}}^{11|12} + G_{\text{Full}}^{22|21} + G_{\text{Full}}^{21|22}), \end{aligned}$$

where we used the definition of the full Green's function $i^2 G_{\text{Full}}^{12|1'2'} = \langle f^1 f^2 f^{2'\dagger} f^{1'\dagger} \rangle$. Since the FRG only calculates the irreducible vertex functions which in turn allow to calculate connected quantities, we have expanded the full Green's function in terms of connected ones [62]

$$G_{\text{Full}}^{12|1'2'} = G_c^{12|1'2'} + G_c^{1|1'} G_c^{2|2'} - G_c^{1|2'} G_c^{2|1'}. \quad (47)$$

These connected Green's functions need further decomposition into the irreducible two-particle vertex function and one-particle Green's functions using the so called tree expansion. The full decomposition is shown in Appendix E.

The dynamical spin structure factor is calculated from the imaginary part of the spin susceptibility via the fluctuation-dissipation theorem as

$$S_{ij}^{\text{Ret}}(\omega) = \frac{1}{\pi} (1 - e^{-\beta\omega})^{-1} \text{Im}(\chi_{ij}^{\text{Ret}}(\omega)). \quad (48)$$

With this we are able to compare our results to inelastic neutron scattering experiments as they are able to directly measure the dynamic spin structure factor.

D. Numerical Implementation

For the implementation of the flow equation we take a route which is similar to state-of-the-art Matsubara implementations [50, 64, 68, 70, 71]. That is, calculating the right hand side of the differential equation exploiting as many symmetries as possible while retaining structures with good ability to be vectorized by the compiler. This means, that we reduce the real space lattice to a minimum set of necessary symmetry in-equivalent points [50] and use the different symmetries from Sec. IV B to remove all negative frequencies by mapping to corresponding Keldysh indices and vertices. The typical approach in PFFRG is to assume an infinite lattice and truncate at a certain interaction distance by setting $\Gamma_{i,j} = 0$ for $\|i - j\| > d_{\text{max}}$ [72].

For the frequency discretization of the two particle vertex we use a linear-logarithmic grid with either 42 or 50 positive frequencies and one additional point at $\omega = 0$. The number of grid points is chosen such that a further increment has no significant impact on the result. The discretization of the self-energy is chosen to be 10 times finer, since the numerical performance loss is insignificant. Further, we use the asymptotic frequency parametrization [73] to correctly capture the asymptotic behavior for the different diagrams. All points in-between grid points are multi-linearly interpolated. To avoid interpolation artifacts, all asymptotic classes have the same frequency discretization. Additionally, we perform a

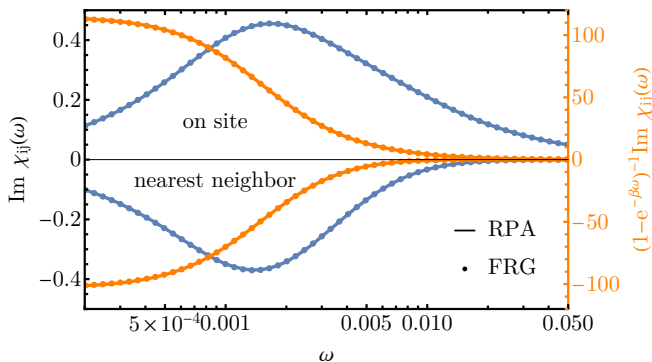


Figure 2. Dynamic susceptibility and resulting spin structure factor [from Eq. (48)] for the antiferromagnetic dimer in the $S \rightarrow \infty$ limit at $T = 0.2J$. The cutoff is chosen such that $\Lambda = 0.002J \ll T$. The results of the FRG coincide with the single step RPA calculation. The spin structure factor shows the expected peak around $\omega = 0$, falling off relatively quickly.

frequency re-meshing of all quantities up to some given cutoff Λ_{\min} using the same interpolation to accurately capture both the large frequency structures at high cutoffs as well as the small frequency features at the end of the flow. The stop of the re-meshing procedure is supported by the re-normalizing behavior of the self-energy, which ensures, that propagator features do not become infinitely sharp. Due to the logarithmic nature of the mesh, this re-meshing sometimes leads to high frequency artifacts, which are also apparent in the RPA analysis shown in Appendix B, but are not significant for the computation of the observables.

For solving the differential equations we use an error-controlled adaptive third order Adams-Bashforth-Moulton stepper [74] which we chose because of the superior performance for FRG in comparison to other steppers [75]. For the frequency integration we opted for a standard adaptive Simpson rule [76] with Richardson extrapolation [77] where we explicitly provide important integration points.

The temperature is implemented into the Fermi distribution which only enters the free Keldysh propagator. This has the consequence that switching from $T = 0$ to $T > 0$ is far simpler compared to the Matsubara formalism, where the frequency integration at $T = 0$ transforms into a discrete sum for $T > 0$. The temperature behavior will be discussed in the next section.

V. RESULTS

To test our technique we analyze a multitude of models for benchmarking purposes. We thus focus on the lower dimensional systems with spatial dimension $D \leq 2$ as there are many numerical, experimental and exact results we can cross-check our results with. This will demonstrate the reliability of the Keldysh PFFRG implementation in comparison to other numerical techniques.

A. Dimer

Since the antiferromagnetic dimer has evolved to be the standard benchmark for PFFRG and PMFRG [28, 51, 56], we use it to compare our technique to the currently available results and extend them to finite frequencies. For this we start with the easier limit, which is $S \rightarrow \infty$, and benchmark against the semi-analytical RPA results. After that, we focus on the full FRG results in the Keldysh formalism and the improvement on the RPA.

1. RPA Results

The dimer is a finite size system both in FRG and RPA. Thus, the results of the FRG at a given cutoff should exactly coincide with the RPA results. The latter are calculated semi-analytically by performing frequency integrals and subsequently inverting the results according to Eq. (29). Since, the RPA calculation scales only linearly with the frequency discretization, we can employ a much finer frequency resolution compared to the FRG approach.

Due to the missing self-energy in the RPA formalism, the temperature plays a crucial role in smoothening the peaked structures. This is necessary, as the frequency resolution would have to be increased significantly to avoid a divergence in the flow for small T with $\Lambda \ll T$ and still resolve all details correctly. In the following we choose $\beta = 5/J$ ($T = 0.2J$) as it is sufficient to show all relevant features when drawing a comparison. Smaller temperatures would necessitate a finer resolution in the FRG part of the calculation, which would be possible in this case but not for the remainder of the paper.

The dynamic susceptibility and the resulting spin structure factor are shown in Fig. 2. At finite temperatures the dynamic susceptibility is constrained to zero by symmetry at $\omega = 0$, leading to peaks at finite ω . To arrive at a less biased quantity we calculate the spin structure factor according to Eq. (48) which leads to the expected behavior around $\omega = 0$, since the classical $S \rightarrow \infty$ limit has gapless excitations and thus a peaked response at $\omega = 0$.

Comparing the FRG results with the RPA data, we can see that the FRG results coincide with the much more accurate RPA scheme. The relative deviations are below 0.3%, which is negligible in comparison to other systematic deviations of the method. A comparison on vertex level further underlines a good performance of the FRG as shown in Appendix B. Thus, we can verify that the FRG is able to resolve the main features during the flow and the frequency resolution of $N_\omega = 50$ is sufficient to approximate the RPA results with $N_\omega = 300$.

2. FRG Results

Following the RPA comparison we now turn to the quantum $S = 1/2$ dimer, where we cannot neglect the remaining parts of the vertex flow and the self-energy also becomes finite. However, due to its simple structure, the antiferromagnetic dimer is exactly solvable, which allows for a good benchmark

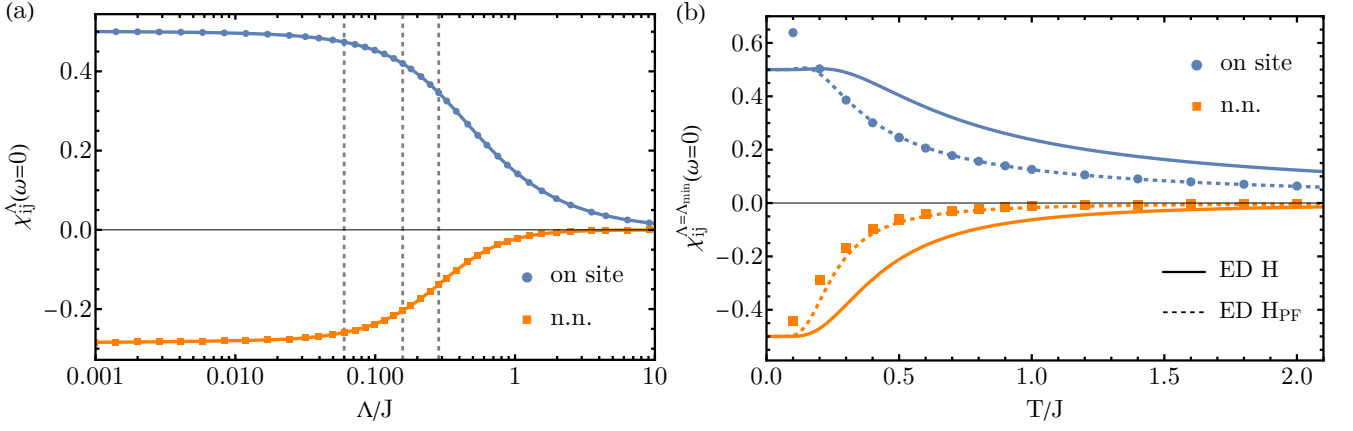


Figure 3. (a) Exemplary FRG flow at $T = 0.2J$ for the antiferromagnetic Heisenberg dimer. The flow exhibits a saturation around $\Lambda = 0.001J$ but is continued down to $\Lambda_{\min} = 10^{-6}J$ to exclude any influence of the cutoff scale. The dashed lines show the cutoffs, which are used for the comparison in Fig. 4. (b) Temperature scaling of the susceptibilities at lowest cutoff Λ_{\min} . The Keldysh PFFRG results match the exact diagonalization results (ED) of the pseudo-fermion dimer down to $T \approx 0.2J$. For smaller T the FRG overestimates the susceptibilities.

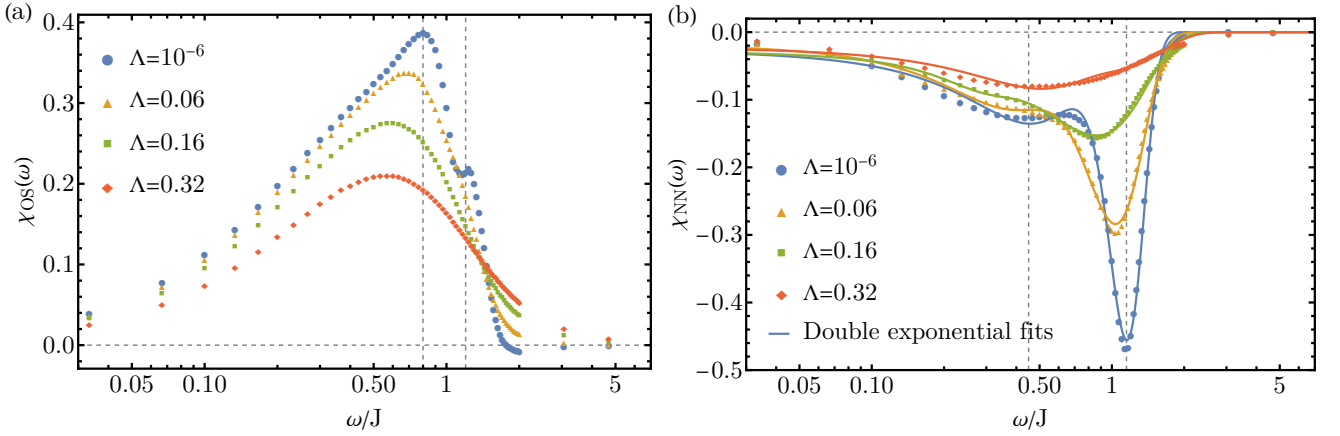


Figure 4. Frequency resolved susceptibilities for the AFM dimer at $T = 0.2J$ for different points in the flow. The chosen cutoffs are also marked in Fig. 3(a). In (b) we also show double exponential fits according to Eq. (51), which describe the susceptibilities up to some minor differences. The peak positions for the smallest cutoffs are marked by dashed lines for better visibility.

of our technique. Since, the FRG calculates susceptibilities, we compare against the exact results for both the physical system ($\chi_{\text{os/nn}}$ for on-site/nearest-neighbor susceptibilities, respectively) as well as the dimer in pseudo-fermion decomposition without projection to the physical subspace ($\chi_{\text{os/nn}}^{\text{pf}}$). This allows us to assess the effect of the pseudo-fermion constraint on our analysis. The exact susceptibilities for $\omega = 0$ are given by

$$\chi_{\text{os}}(\beta) = \frac{\beta + e^\beta - 1}{2e^{\beta/4} Z_{\text{ph}}(\beta)}, \quad \chi_{\text{nn}}(\beta) = \frac{\beta - e^\beta + 1}{2e^{\beta/4} Z_{\text{ph}}(\beta)}, \quad (49)$$

$$\chi_{\text{os}}^{\text{pf}}(\beta) = \frac{\beta + e^\beta - 1 + 2\beta e^{\beta/4}}{2e^{\beta/4} Z_{\text{pf}}(\beta)}, \quad \chi_{\text{nn}}^{\text{pf}}(\beta) = \frac{\beta - e^\beta + 1}{2e^{\beta/4} Z_{\text{pf}}(\beta)},$$

$$e^{\beta/4} Z_{\text{ph}}(\beta) = e^\beta + 3, \quad e^{\beta/4} Z_{\text{pf}}(\beta) = e^\beta + 3 + 12e^{\beta/4}.$$

These quantities can be calculated using the Lehmann representation [51] which is laid out in Appendix F.

We perform the FRG calculations with $N_\omega = 50$ for different temperatures. For $T > 0.1J$ we get a monotonous flow down to the smallest cutoff Λ , which we set to $\Lambda_{\min} = 10^{-6}J$ to avoid any effects that a finite cutoff could have on the results. This can be done in the FRG since the self-energy regularizes the divergence and, thus, sharp peaks, which appeared in the RPA, are avoided. An exemplary flow of the on-site and nearest-neighbor susceptibility at $\omega = 0$ is depicted in Fig. 3(a). It illustrates that the results are already cutoff independent for $\Lambda < 0.01J$ as the flow saturates.

The final values of the susceptibilities for each temperature are depicted in Fig. 3(b). It shows that for $T > 0.2J$ the results match with the exact pseudo-fermion solution but not the exact dimer. This discrepancy arises because we only assume the constraint Eq. (4) to be fulfilled on average. Therefore, we allow the unphysical states to enter the results. As can be seen from Eqs. (49) these mainly results in the change of the partition function by a constant term. Only in the on-site susceptibility there is a possibility for an unphysical state to play

a role in the expectation value, but this is also only for $\omega = 0$. Thus, we would assume that the pseudo-fermion constraint does not impact the results more than change their scaling. Unfortunately, this reasoning is only valid for a FRG without truncation, as the truncation in principle allows for the unphysical behavior to be enhanced. This issue was already discussed by Schneider *et al.* [49] who used the Popov-Fedotov technique [47, 48] to project out the unphysical states in the partition function by applying an imaginary chemical potential. However, this removes the symmetry of the vertex under complex conjugation and thus further increases the numerical effort. As the Keldysh PFFRG is already numerically expensive, we decided against employing this technique in this study. A more suitable approach would be to implement the Keldysh formalism into the pseudo Majorana FRG as it does not have the drawback of violating the particle number constraint.

Moreover, the FRG tends to exhibit ordering behavior, even in scenarios where it would be prohibited by the Mermin-Wagner theorem. This phenomenon is observed for the dimer at $T = 0.1J$, where the flow shows a small plateau in the nearest neighbor susceptibility instead of remaining monotonous [see App. C]. This suggests that the system is attempting to transition away from the disordered paramagnetic starting state, which in turn renders the FRG flow unstable. Consequently, we refrain from continuing the analysis below $T = 0.1J$ for the dimer.

Additional deviations can be attributed to the truncation of the FRG equations. In our analysis, we truncated at the one-loop level, which effectively neglects three-particle contributions. The Katanin substitution [61] provides partial compensation for this omission, but higher-order terms still remain unaccounted for in the FRG flow. Unfortunately, this truncation can introduce uncontrollable effects, leading to a flow that is cutoff-dependent rather than cutoff-universal [57]. As a result, using the FRG as a quantitative tool becomes problematic when higher-order terms cannot be excluded. Although extending the method to include higher-loop terms appears promising, the benefits may not justify the exponentially increased computational cost [70]. Nonetheless, the qualitative predictions of PFFRG have already proven reliable for one-loop calculations, with increasing accuracy in higher-dimensional systems [25, 26, 28, 78–87]. The zero-dimensional dimer, therefore, serves as a benchmark with the potentially severest qualitative issues.

Unphysical excitations are also apparent in the frequency spectrum of both in-equivalent dimer sites, as illustrated in Fig. 4 for $T = 0.2J$. A double peak structure is observed in both the on-site and nearest neighbor susceptibilities. However, from the exact result

$$\chi_{\text{os/nn}}^{(\text{pf})}(\omega) \propto \lim_{\eta \rightarrow 0} \pm \left(\frac{1}{\omega + i\eta - J} - \frac{1}{\omega + i\eta + J} \right) \quad (50)$$

we would expect only a single peak for $\omega > 0$ in the imaginary part of the susceptibility exactly at $\omega = J$, as this is the energy required to induce a spin flip from the ground state. Thus, we identify the largest peak in the nearest neighbor susceptibility

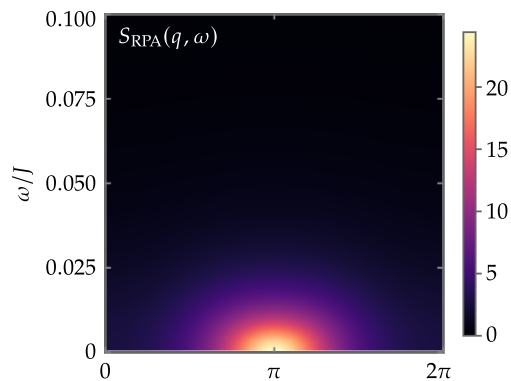


Figure 5. Spin structure factor for the spin chain with $N = 10$ in the $S \rightarrow \infty$ limit. The excitation is localized around $q = \pi$ and falls off quickly for $\omega > 0$. We do not get any branches, as we would get in spin wave theory since the initial state in the FRG is fully disordered and thus paramagnetic .

as the physical excitation.

We perform a fit of the nearest-neighbor susceptibility according to

$$\chi_{\text{NN,Fit}}(\omega) = A_1 e^{-\frac{1}{2} \frac{(\omega - \omega_1)^2}{\sigma_1^2}} + A_2 e^{-\frac{1}{2} \frac{(\omega - \omega_2)^2}{\sigma_2^2}}, \quad (51)$$

also shown in Fig. 4(b).

We find, that there is a deviation of the main peak from the expected value of $\omega = J$. We find, that the peak is found at $\omega < J$ for both higher temperatures and cutoffs, shifting towards J upon lowering any two of these, and eventually reaching $\omega > J$ for low temperatures and cutoffs. This deviation as well as the additional peak we attribute to the inherent approximations of PFFRG. As evident from the varying cutoff values Λ , the broadening is also significantly amplified by the cutoff scale. Therefore, only in the case of $\Lambda \ll T$ can we reasonably assume that the results do not exhibit any additional broadening beyond the truncation effects and temperature broadening. For the on-site susceptibility, a double exponential fit failed to accurately describe the data points.

Based on this analysis of the dimer and the pseudo-fermion constraint, we will limit our investigation to $T = 0.1J$ as the lowest temperature value, aligning with typical PFFRG boundaries [49], provided, the flow exhibits a monotonous behavior. However, selecting the smallest possible temperature is encouraged, as temperature broadening tends to obscure distinct features. Additionally, we acknowledge that certain modes may not exhibit the correct physical behavior, though we expect these modes to be small compared to the physically relevant ones, as seen for the nearest neighbor susceptibility.

B. 1D Spin Chain

From the zero-dimensional dimer we now shift focus to the one-dimensional spin chain with nearest (J_1) and next-nearest (J_2) neighbor AFM interactions.

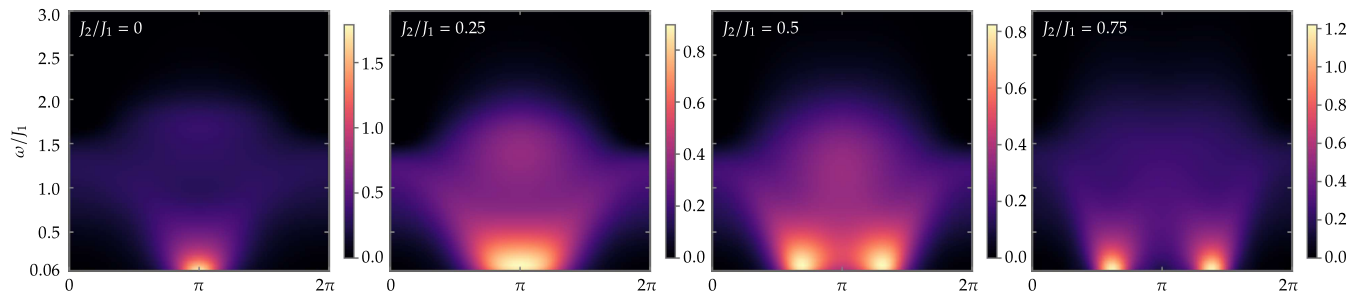


Figure 6. Dynamical spin structure factor for the one-dimensional spin chain with $l = 10$ at $T = 0.1J_1$. For $J_2/J_1 = 0$ we can see a strong peak at $q = \pi$. The spinon continuum is visible above the main excitation. For $J_2/J_1 > J_{KT}$ we should see a gapped spectrum, which is not visible in our results. For larger J_2/J_1 we get a splitting of the main peak into two peaks.

1. RPA results

Similar to the AFM dimer we first discuss the results in the classical $S \rightarrow \infty$ limit. The RPA results – coinciding with the FRG – are shown in Fig. 5. Excitations are observable only for $\omega \approx 0$ with a maximum at $q = \pi$. However, we would expect excitation branches for all q with a notable dispersion in ω , since the classical $S \rightarrow \infty$ limit should be well described by linear spin wave theory (SWT) [88, 89]. There, in first order, the dispersion is given by

$$\omega \propto J|\sin(q)|, \quad \text{with } q \in \{0, 2\pi\}. \quad (52)$$

However, this holds only under the assumption of a response around an ordered ground state, which is in contrast to the FRG where one assumes the initial state to be paramagnetic and thus maximally disordered [29]. As outlined above, achieving magnetic order in the FRG would require the presence of a finite order parameter within the flow. Since, we exclude any magnetic order parameter, the flow diverges in the vicinity of any ordering phase, confining us to the paramagnetic regime. This limitation may also explain why small temperatures cannot be reached in the RPA calculations since the t -channel is known to enhance the ordering tendencies, while the $-$ in the RPA vanishing $-s$ and u channel suppress ordering [50, 90]. Without a flowing order parameter, the divergence reflects the onset of ordering. This observation also sets the stage for the remainder of this study, as systems well-described by SWT may lack certain features in FRG, especially around $q = 0$. As mentioned above, to permit a flow into the symmetry broken phase, the Keldysh PFFRG would have to allow for a magnetic field, which induces a spin rotational symmetry breaking.

2. FRG results

Following the RPA discussion we now focus on the full FRG solution and analyze how the additional channels and the interplay between them enhances the results to be able to describe the full quantum $S = 1/2$ Heisenberg model.

When analyzing this model one normally expects the typical excitations to carry spin $S = 1$ which are the so-called

magnons. For spin liquids however, it is possible for the system to exhibit $S = 1/2$ spinons as the principal excitation, which implies a fractionalization of the spin quantum number [92]. In the case of the spin chain these can be identified with domain walls, which can propagate freely through the chain once they are created until they are annihilated again. Thus, calculating the spin structure factor for the Heisenberg spin chain is an excellent test of our method to ascertain whether emergent excitations can be resolved. Furthermore, the J_1 - J_2 phase diagram is already well studied and can be used as a benchmark [93]. Specifically, for $J_2 = 0$ we have the isotropic spin chain, which is exactly solvable using the Bethe Ansatz [94]. At the Kosterlitz-Thouless point $J_2/J_1 = J_{KT} = 0.24116(7)$ [95] the system exhibits a phase transition from gapless to gapped [93].

For $J_2/J_1 = 0.5$ the system is known as the Majumdar-Ghosh model [96] which akin to the $J_2 = 0$ case is analytically solvable. Lastly, for $J_2 \rightarrow \infty$ the system transitions into two decoupled spin chains, which closes the gap again. The results for the intermediate values can be compared against various numerical techniques as the variational Monte Carlo approach [97, 98] and also experimental data [99].

We calculate the dynamical spin structure factor for correlations up to $l = 10$ sites with different J_2/J_1 at $T = 0.1J_1$. The temperature was chosen as a compromise between $T \ll J_1$ and the effects described in Sec. V A. The resulting spectra are shown in Fig. 6. Since, $\text{Im}(\chi(\omega = 0)) = 0$ is given by symmetry we only show the values for $\omega > 0$, as the limit $\omega \rightarrow 0$ in the structure factor Eq. (48) is ill-defined. The smallest frequency we use is $\omega = 0.06$. This choice is arbitrary and results from the susceptibility calculation discretization. For larger ω , some susceptibilities are slightly smaller than zero. We attribute this to numerical inaccuracies and set those values to zero since they are at least two orders of magnitude smaller compared to the results for small frequencies.

All structure factors show the typical dome structure as well as the spinon continuum. Below the Majumdar-Ghosh point we get one maximum at $q = \pi$. In this phase one would also expect branches going down to $q = 0$ as discussed in Sec. V B 1. However, this is not resolved in our analysis as the susceptibility continuously decreases away from $q = \pi$. This means, that the additional channels cannot remedy the fact, that the paramagnetic phase which we cannot leave during the

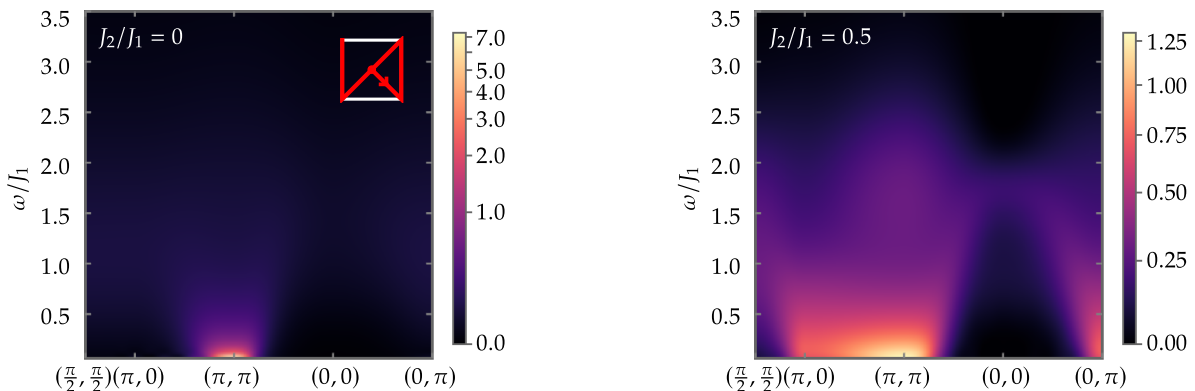


Figure 7. Dynamical spin structure factor for the square lattice at $T = 0.1J_1$ with a maximum distance of $l = 7$ lattice sites along the depicted high symmetry line. $J_2 = 0$ is the unfrustrated case and is taken at $\Lambda = 0.48J_1$, as the flow had to be stopped due to the ordering tendencies. The sharp peak at $\mathbf{q} = (\pi, \pi)$ signals the antiferromagnetic ordering. Due to the large cutoff scale sharp branches are not visible. For the frustrated case with $J_2/J_1 = 0.5$ we see a strong signal also at $\mathbf{q} = (\pi, 0)$ which is to be expected [91]. In both cases the branch to $\mathbf{q} = (0, 0)$ is not resolved.

flow, suppresses these kind of branches.

Further, a differentiation between gapless and gapped spectra is not possible because only the $J_2 = 0$ spectrum should be gapless. For $J_2/J_1 \leq 0.5$, our inability to resolve the gap could be attributed to its relatively small sizes and the finite temperatures in our calculations but for $J_2/J_1 = 0.75$ the gap is $\Delta/J_1 \approx 0.4$ [93], which should be well resolved. Thus we can argue, that the Keldysh-PFFRG is not able to resolve the difference between a gapped and a gapless spectrum. This is again due to the nature of FRG, as we need a finite mass term for the excitations to create a gap in the spectrum. This mass term however is connected to the order parameter of an ordered phase and would need to be specifically included into the flow to become finite. Otherwise it is just neglected, which is why our implementation is not able to differentiate between gapped and gapless spectra.

At $J_2 = 0.5J_1$, the exactly-solvable Majumdar-Ghosh point, we find incommensurate correlations for $\omega \rightarrow 0$. Analytically, the dominant correlations should still reside at $q = \pi$ and only for larger J_2 move towards $q = \pi/2$. This finding, however, is consistent with Matsubara PFFRG calculations using the `PFFRGsolver.jl` software [70, 100], where we find the exact same values of q for the dominant correlations. For $J_2/J_1 > 0.5$ we, however, see the correct behavior of the system, which means a continuous movement of the peak position to $q = \pi/2$. Also, the peak intensity of the susceptibility at $J_2/J_1 = 0.75$ shows the trend of transforming into two decoupled spin chains as found for $J_2 \rightarrow \infty$.

This means, that PFFRG is able to qualitatively resemble the structure of the features in the susceptibility and improve significantly beyond the results of the RPA calculation, which was merely able to reflect the paramagnetic properties of the initial state. Nevertheless, the inability of our method to enter a symmetry broken phase still prohibits some features as well as a proper quantitative analysis for the FRG.

C. (Frustrated) Square Lattice

Having discussed zero- and one-dimensional system, we now turn our attention to the two-dimensional square lattice. For only nearest-neighbor antiferromagnetic interactions the system is known to have a Néel-ordered ground state with ordering vector $\mathbf{q} = (\pi, \pi)$ at $T = 0$. The elementary excitations can be described by spin wave theory and are gapless. In first order SWT the dispersion is given by

$$\omega \propto J\sqrt{1 - \gamma(\mathbf{q})^2}, \quad \text{with } 2\gamma(\mathbf{q}) = \cos(q_x) + \cos(q_y). \quad (53)$$

Note, that there are additional modulations when computing the spin susceptibility, which suppress the intensity around $q = (0, 0)$. While higher-order corrections to this result can be computed [102], it is important to note that spin wave theory, being a semiclassical approach, fails to account for certain deviations, particularly a suppression of spectral weight at $\mathbf{q} = (\pi, 0)$ [103]. These deviations, however, are captured by a series expansion approach [104, 105].

We analyze the square lattice with a maximal correlation length of $l = 7$ for both the pure nearest-neighbor antiferromagnet and a parametrically frustrated parameter point with next-nearest neighbor coupling $J_2 = 0.5J_1$. In the pure nearest-neighbor model ($J_2 = 0$) we encounter a divergence in the flow signaling an ordered ground state. This should in principle not be the case because the Mermin-Wagner theorem prohibits breaking of the continuous spin-rotation symmetry in two dimensions for $T > 0$. The PFFRG however, especially at low temperatures, shows enhanced ordering tendencies, which result in the divergence as already discussed in Sec. V A. To avoid this, we could have performed the calculations at a higher temperature, where there would be no divergence in the flow (i.e. $T \approx J$). This approach, though, would significantly smear out all signatures in the dynamic structure factor. Thus, we stay at $T = 0.1J$ considering that the $J_2 = 0$ case should only be taken as a reference for the frustrated parameters. The resulting spin structure factors are

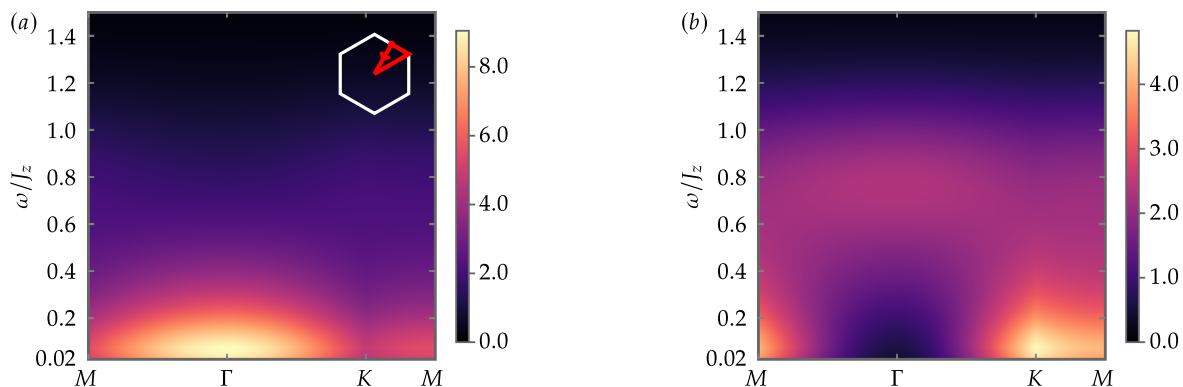


Figure 8. Dynamical spin structure factor for the isotropic Honeycomb-Kitaev model at $\beta = 10/J$. The ferromagnetic (a) and the anti-ferromagnetic (b) case show the typical excitation structure of the Kitaev model. The high symmetry path is chosen to match Ref. [101] and is depicted in (a). The frequency scale does not match the exact results and the two-flux gap is not resolved.

shown in Fig. 7. When comparing these results to VMC [91] or other numerical approaches [106–110] we observe a qualitatively good agreement, except for the branches leading to $\mathbf{q} = (0, 0)$ – an issue also encountered in the one-dimensional spin chain. This we again attribute to the paramagnetic nature of the FRG flow. Nonetheless, within the frustrated regime, the PFFRG successfully captures the gapless excitations at $(\pi, 0)$ and $(0, \pi)$ for $J_2/J_1 = 0.5$, which can be ascribed to the gapless \mathbb{Z}_2 Dirac spin liquid ground state (the Z2Azz13 state of Ref. [19]) in this region, which features four Dirac cones at $(\pm\frac{\pi}{2}, \pm\frac{\pi}{2})$ in the spinon spectrum resulting in gapless two-spinon excitations at $(\pi, 0)$ and $(0, \pi)$ in addition to the ones at $(0, 0)$ and (π, π) [91, 110]. The missing arc between $\mathbf{q} = (\pi, 0)$ and (π, π) in the frustrated case could be due to the one-loop implementation of the PFFRG but also because of the relatively strong broadening due to the temperature. Nevertheless, the comparison between the frustrated and the non-frustrated model shows a clear formation of an excitation continuum in the frustrated case, while the excitations remain relatively localized for $J_2 = 0$. There however, clear branches are absent due to the divergence of the flow, leading to the evaluation of the susceptibility at finite Λ , which introduces broadening and obscures any clear dispersion or even formation of spinon branches.

Most importantly, in the spin liquid regime, we are able to resolve the spinon continuum, and successfully describe the development of gapless excitations at $(0, \pi)$ and $(\pi, 0)$ characterizing the nature of the spin liquid, while the missing branches out of $\mathbf{q} = (0, 0)$ and between $\mathbf{q} = (\pi, 0)$ and $\mathbf{q} = (\pi, \pi)$ are most likely not captured due to finite temperature effects. Thus, we can support the claim, that higher dimensional systems are more favorable to the FRG formalism, as approaching the critical mean-field dimension $n = 4$ reduces the effect of non-renormalizable large local couplings [111].

D. Honeycomb-Kitaev model

Going beyond the isotropic Heisenberg model, we introduce directional couplings J^{xx} , J^{yy} and J^{zz} in spin space, which allow us to calculate the dynamical spin structure factor of a much larger class of magnetic systems. We chose the Honeycomb-Kitaev model as a benchmark, as it is analytically solvable via the introduction of Majorana fermions [101, 112]. The Kitaev-Honeycomb model is defined on a typical honeycomb lattice with interactions chosen such that only one of the J^{aa} is non-zero along a specific bond direction [113].

Further, the Kitaev-Honeycomb model suits the PFFRG as one can show that only nearest-neighbor interactions play a role in the flow and we thus can calculate the dynamics with very small numerical effort. The dynamical spin structure factors for the isotropic ferromagnetic and anti-ferromagnetic interactions are depicted in Fig. 8. Both resemble the structure of the exact solution given in Ref. [101]. In the ferromagnetic case, we find a broad spectrum at low frequency, which is lightly peaked around the Γ point with a continuum of excitations which falls off quickly for larger frequencies. In the antiferromagnetic case, the structure factor is peaked at the K point at small frequencies and shows vanishing spectral weight in a region around Γ . At higher energies, this spectral gap is arched over by a continuum in the structure factor, as found in the analytical solution. However, in both cases, the two-flux gap is not visible. This again is due to the fact, that the FRG is not able to resolve gapped spectra without the inclusion of an additional flowing order parameter. Further, the energy scale of the PFFRG results is approximately five times smaller than the corresponding exact results which might also be a result of the missing order parameter or is due to the paramagnetic starting point of our technique. This benchmark shows, that our approach is only able to give correct qualitative results, but quantitatively lacks in comparability.

VI. CONCLUSION

The Keldysh formulation of the pseudo-fermion functional renormalization group (FRG) stands out as a novel many-body framework capable of directly evaluating dynamic spin structure factors of spin models in an unbiased way. We have benchmarked our technique for low-dimensional spin models with diagonal interactions such as the zero-dimensional dimer, the one-dimensional spin chain, and the two-dimensional square lattice (also with frustrated interactions) Heisenberg models. Furthermore, we assessed the dynamical spin structure factor for the canonical Kitaev-Honeycomb model for which exact results are available. As expected the Keldysh PFFRG results significantly improve upon those from RPA and seem particularly reliable for systems with an absence of conventional magnetic order. It would constitute an important future endeavor to allow for inclusion of Zeeman pinning fields in the Keldysh formulation of PFFRG which would permit a flow into the ordered phase without encountering unphysical divergencies in the flow down till zero cutoff, and thus enabling us to faithfully capture magnon branches. Therefore, the presently developed Keldysh PFFRG is best suited for models in the highly frustrated regime displaying putative spin liquid behavior close to the paramagnetic regime, which is indeed the regime of interest where most pressing questions at the interface with quantum materials lie. While factors such as pseudo-fermion number violation, the paramagnetic initial state and finite-temperature effects limit the quantitative accuracy of the Keldysh PFFRG results, we believe that this work opens pathways to further refinements which mitigate these factors, and will thus potentially make it a sharpened tool for exploring the intricate excitation spectra of models and materials. These pathways include - as mentioned in the main text - employing the pseudo-Majorana decomposition [51, 52], incorporating the Popov-Fedotov technique, and extending the flow to account for non-zero mag-

netic fields [68, 69]. Also, increasing the numerical performance should lead to the possibility of scanning phase diagrams instead of singular phase space points. Further, using the full Keldysh formalism [32, 114] will allow for accessing non-equilibrium phenomena in frustrated magnets such as computation of spinon currents and transport coefficients, which remain *terra incognita*. Given the arrival of a plethora of three-dimensional candidate quantum spin liquid materials based on novel lattices of spin-1/2 and 1 magnetic moments for which neutron scattering profiles are currently getting available, the Keldysh PFFRG approach would serve as a valuable tool in identifying the precise nature of the spin liquids by making connections to the underlying microscopic model.

VII. ACKNOWLEDGEMENTS

We thank Nils Niggemann and Johannes Reuther for fruitful discussions. We also want to thank Anxiang Ge and Nepomuk Ritz for benchmarking the Keldysh implementation against the SIAM code. Further we want to explicitly thank Benedikt Schneider for highlighting a problem in the susceptibility calculation. The work is funded by the Deutsche Forschungsgemeinschaft (DFG, German Research Foundation) through Project-ID 258499086 - SFB 1170, through the Würzburg-Dresden Cluster of Excellence on Complexity and Topology in Quantum Matter – *ct.qmat* Project-ID 390858490 - EXC 2147 and the Research Unit QUAST by the DFG Project-ID 449872909 - FOR5249. The work of Y.I. was performed in part at the Aspen Center for Physics, which is supported by National Science Foundation Grant No. PHY-2210452 and a grant from the Simons Foundation (1161654, Troyer). This research was supported in part by grant NSF PHY-2309135 to the Kavli Institute for Theoretical Physics (KITP). Y.I. acknowledges support from the ICTP through the Associates Programme and from the Simons Foundation through Grant No. 284558FY19.

-
- [1] J. R. Chamorro, T. M. McQueen, and T. T. Tran, Chemistry of Quantum Spin Liquids, *Chem. Rev.* **121**, 2898 (2021).
 - [2] B. Binz and A. Vishwanath, Theory of helical spin crystals: Phases, textures, and properties, *Phys. Rev. B* **74**, 214408 (2006).
 - [3] S. Mühlbauer, B. Binz, F. Jonietz, C. Pfleiderer, A. Rosch, A. Neubauer, R. Georgii, and P. Böni, Skyrmion Lattice in a Chiral Magnet, *Science* **323**, 915 (2009).
 - [4] N. Nagaosa and Y. Tokura, Topological properties and dynamics of magnetic skyrmions, *Nat. Nanotechnol.* **8**, 899 (2013).
 - [5] Y. Fujishiro, N. Kanazawa, T. Nakajima, X. Z. Yu, K. Ohishi, Y. Kawamura, K. Kakurai, T. Arima, H. Mitamura, A. Miyake, K. Akiba, M. Tokunaga, A. Matsuo, K. Kindo, T. Koretsune, R. Arita, and Y. Tokura, Topological transitions among skyrmion- and hedgehog-lattice states in cubic chiral magnets, *Nat. Commun.* **10**, 1059 (2019).
 - [6] L. Messio, C. Lhuillier, and G. Misguich, Lattice symmetries and regular magnetic orders in classical frustrated antiferromagnets, *Phys. Rev. B* **83**, 184401 (2011).
 - [7] M. Gembé, H.-J. Schmidt, C. Hickey, J. Richter, Y. Iqbal, and S. Trebst, Noncoplanar magnetic order in classical square-kagome antiferromagnets, *Phys. Rev. Res.* **5**, 043204 (2023).
 - [8] M. Gembé, L. Gresista, H.-J. Schmidt, C. Hickey, Y. Iqbal, and S. Trebst, Noncoplanar orders and quantum disordered states in maple-leaf antiferromagnets, *Phys. Rev. B* **110**, 085151 (2024).
 - [9] P. Santini, S. Carretta, G. Amoretti, R. Caciuffo, N. Magnani, and G. H. Lander, Multipolar interactions in *f*-electron systems: The paradigm of actinide dioxides, *Rev. Mod. Phys.* **81**, 807 (2009).
 - [10] Y. Kuramoto, H. Kusunose, and A. Kiss, Multipole Orders and Fluctuations in Strongly Correlated Electron Systems, *J. Phys. Soc. Jpn.* **78**, 072001 (2009).
 - [11] A. F. Andreev and I. A. Grishchuk, Spin nematics, *JETP Lett.* **60**, 267 (1984).

- [12] R. Sibille, N. Gauthier, E. Lhotel, V. Porée, V. Pomjakushin, R. A. Ewings, T. G. Perring, J. Ollivier, A. Wildes, C. Ritter, T. C. Hansen, D. A. Keen, G. J. Nilsen, L. Keller, S. Petit, and T. Fennell, A quantum liquid of magnetic octupoles on the pyrochlore lattice, *Nat. Phys.* **16**, 546 (2020).
- [13] H. Ikeda, M.-T. Suzuki, R. Arita, T. Takimoto, T. Shibauchi, and Y. Matsuda, Emergent rank-5 nematic order in URu₂Si₂, *Nat. Phys.* **8**, 528 (2012).
- [14] J. A. M. Paddison, H. Jacobsen, O. A. Petrenko, M. T. Fernández-Díaz, P. P. Deen, and A. L. Goodwin, Hidden order in spin-liquid Gd₃Ga₅O₁₂, *Science* **350**, 179 (2015).
- [15] A. Smerald and N. Shannon, Theory of spin excitations in a quantum spin-nematic state, *Phys. Rev. B* **88**, 184430 (2013).
- [16] Y. Kato, S. Hayami, and Y. Motome, Spin excitation spectra in helimagnetic states: Proper-screw, cycloid, vortex-crystal, and hedgehog lattices, *Phys. Rev. B* **104**, 224405 (2021).
- [17] L. Savary and L. Balents, Quantum spin liquids: a review, *Rep. Prog. Phys.* **80**, 016502 (2016).
- [18] C. Broholm, R. J. Cava, S. A. Kivelson, D. G. Nocera, M. R. Norman, and T. Senthil, Quantum spin liquids, *Science* **367**, eaay0668 (2020).
- [19] X.-G. Wen, Quantum orders and symmetric spin liquids, *Phys. Rev. B* **65**, 165113 (2002).
- [20] F. Ferrari and F. Becca, Dynamical Structure Factor of the $J_1 - J_2$ Heisenberg Model on the Triangular Lattice: Magnons, Spinons, and Gauge Fields, *Phys. Rev. X* **9**, 031026 (2019).
- [21] F. Ferrari and F. Becca, Spectral signatures of fractionalization in the frustrated Heisenberg model on the square lattice, *Phys. Rev. B* **98**, 100405 (2018).
- [22] R. G. Pereira, J. Sirker, J.-S. Caux, R. Hagemans, J. M. Maillet, S. R. White, and I. Affleck, Dynamical Spin Structure Factor for the Anisotropic Spin-1/2 Heisenberg Chain, *Phys. Rev. Lett.* **96**, 257202 (2006).
- [23] N. E. Sherman, M. Dupont, and J. E. Moore, Spectral function of the $J_1 - J_2$ Heisenberg model on the triangular lattice, *Phys. Rev. B* **107**, 165146 (2023).
- [24] M. Drescher, L. Vanderstraeten, R. Moessner, and F. Pollmann, Dynamical signatures of symmetry-broken and liquid phases in an $S = \frac{1}{2}$ Heisenberg antiferromagnet on the triangular lattice, *Phys. Rev. B* **108**, L220401 (2023).
- [25] M. G. Gonzalez, V. Noculak, A. Sharma, V. Favre, J.-R. Soh, A. Magrez, R. Bewley, H. O. Jeschke, J. Reuther, H. M. Rønnow, Y. Iqbal, and I. Živković, Dynamics of K₂Ni₂(SO₄)₃ governed by proximity to a 3D spin liquid model, *Nat. Commun.* **15**, 7191 (2024).
- [26] S. Chillal, Y. Iqbal, H. O. Jeschke, J. A. Rodriguez-Rivera, R. Bewley, P. Manuel, D. Khalyavin, P. Steffens, R. Thomale, A. T. M. N. Islam, J. Reuther, and B. Lake, Evidence for a three-dimensional quantum spin liquid in PbCuTe₂O₆, *Nat. Commun.* **11**, 2348 (2020).
- [27] K. W. Plumb, H. J. Changlani, A. Scheie, S. Zhang, J. W. Krizan, J. A. Rodriguez-Rivera, Y. Qiu, B. Winn, R. J. Cava, and C. L. Broholm, Continuum of quantum fluctuations in a three-dimensional $S = 1$ Heisenberg magnet, *Nat. Phys.* **15**, 54 (2019).
- [28] T. Müller, D. Kiese, N. Niggemann, B. Sbierski, J. Reuther, S. Trebst, R. Thomale, and Y. Iqbal, Pseudo-fermion functional renormalization group for spin models, *Rep. Prog. Phys.* **87**, 036501 (2024).
- [29] J. Reuther and P. Wölfle, $J_1 - J_2$ frustrated two-dimensional Heisenberg model: Random phase approximation and functional renormalization group, *Phys. Rev. B* **81**, 144410 (2010).
- [30] A. Kamenev, *Field Theory of Non-Equilibrium Systems* (Cambridge University Press, 2011).
- [31] S. G. Jakobs, M. Pletyukhov, and H. Schoeller, Nonequilibrium functional renormalization group with frequency-dependent vertex function: A study of the single-impurity Anderson model, *Phys. Rev. B* **81**, 195109 (2010).
- [32] S. G. Jakobs, V. Meden, and H. Schoeller, Nonequilibrium Functional Renormalization Group for Interacting Quantum Systems, *Phys. Rev. Lett.* **99**, 150603 (2007).
- [33] L. M. Sieberer, M. Buchhold, and S. Diehl, Keldysh field theory for driven open quantum systems, *Rep. Prog. Phys.* **79**, 096001 (2016).
- [34] C. Fräßdorf and J. E. M. Mosig, Keldysh functional renormalization group for electronic properties of graphene, *Phys. Rev. B* **95**, 125412 (2017).
- [35] A. Ge, N. Ritz, E. Walter, S. Aguirre, J. von Delft, and F. B. Kugler, Real-frequency quantum field theory applied to the single-impurity Anderson model, *Phys. Rev. B* **109**, 115128 (2024).
- [36] N. Ritz, A. Ge, E. Walter, S. Aguirre, J. von Delft, and F. B. Kugler, KeldyshQFT: A C++ codebase for real-frequency multiloop functional renormalization group and parquet computations of the single-impurity Anderson model (2024), [arXiv:2405.20996 \[cond-mat.str-el\]](https://arxiv.org/abs/2405.20996).
- [37] J. Reuther and R. Thomale, Cluster functional renormalization group, *Phys. Rev. B* **89**, 024412 (2014).
- [38] J. Krieg and P. Kopietz, Exact renormalization group for quantum spin systems, *Phys. Rev. B* **99**, 060403 (2019).
- [39] D. Tarasevych, J. Krieg, and P. Kopietz, A rich man's derivation of scaling laws for the Kondo model, *Phys. Rev. B* **98**, 235133 (2018).
- [40] R. Goll, D. Tarasevych, J. Krieg, and P. Kopietz, Spin functional renormalization group for quantum Heisenberg ferromagnets: Magnetization and magnon damping in two dimensions, *Phys. Rev. B* **100**, 174424 (2019).
- [41] R. Goll, A. Rückriegel, and P. Kopietz, Zero-magnon sound in quantum Heisenberg ferromagnets, *Phys. Rev. B* **102**, 224437 (2020).
- [42] D. Tarasevych and P. Kopietz, Dissipative spin dynamics in hot quantum paramagnets, *Phys. Rev. B* **104**, 024423 (2021).
- [43] D. Tarasevych and P. Kopietz, Critical spin dynamics of Heisenberg ferromagnets revisited, *Phys. Rev. B* **105**, 024403 (2022).
- [44] A. Rückriegel, J. Arnold, R. Goll, and P. Kopietz, Spin functional renormalization group for dimerized quantum spin systems, *Phys. Rev. B* **105**, 224406 (2022).
- [45] A. Rückriegel, D. Tarasevych, and P. Kopietz, Phase diagram of the $J_1 - J_2$ quantum Heisenberg model for arbitrary spin, *Phys. Rev. B* **109**, 184410 (2024).
- [46] A. A. Abrikosov, Electron scattering on magnetic impurities in metals and anomalous resistivity effects, *Physique Physique Fizika* **2**, 5 (1965).
- [47] V. N. Popov and S. Fedotov, The functional integration method and diagram technique for spin systems, *Zh. Eksp. Teor. Fiz* **94**, 183 (1988).
- [48] N. V. Prokof'ev and B. V. Svistunov, From the Popov-Fedotov case to universal fermionization, *Phys. Rev. B* **84**, 073102 (2011).
- [49] B. Schneider, D. Kiese, and B. Sbierski, Taming pseudo-fermion functional renormalization for quantum spins: Finite temperatures and the Popov-Fedotov trick, *Phys. Rev. B* **106**, 235113 (2022).
- [50] J. Reuther, *Frustrated Quantum Heisenberg Antiferromagnets: Functional Renormalization-Group Approach in Auxiliary-Fermion Representation*, Ph.D. thesis, Karlsruhe Institut für Technologie (KIT) (2011).

- [51] N. Niggemann, B. Sbierski, and J. Reuther, Frustrated quantum spins at finite temperature: Pseudo-Majorana functional renormalization group approach, *Phys. Rev. B* **103**, 104431 (2021).
- [52] N. Niggemann, J. Reuther, and B. Sbierski, Quantitative functional renormalization for three-dimensional quantum Heisenberg models, *SciPost Phys.* **12**, 156 (2022).
- [53] L. V. Keldysh, Diagram technique for nonequilibrium processes, *Zh. Eksp. Teor. Fiz* **47**, 151 (1964).
- [54] K. G. Wilson, The renormalization group: Critical phenomena and the Kondo problem, *Rev. Mod. Phys.* **47**, 773 (1975).
- [55] C. Taranto, S. Andergassen, J. Bauer, K. Held, A. Katanin, W. Metzner, G. Rohringer, and A. Toschi, From Infinite to Two Dimensions through the Functional Renormalization Group, *Phys. Rev. Lett.* **112**, 196402 (2014).
- [56] B. Schneider, J. Reuther, M. G. Gonzalez, B. Sbierski, and N. Niggemann, Temperature flow in pseudo-Majorana functional renormalization for quantum spins, *Phys. Rev. B* **109**, 195109 (2024).
- [57] S. G. Jakobs, *Functional renormalization group studies of quantum transport through mesoscopic systems*, Ph.D. thesis, Aachen, Techn. Hochsch., Diss., 2009 (2009).
- [58] S. G. Jakobs, M. Pletyukhov, and H. Schoeller, Properties of multi-particle Green's and vertex functions within Keldysh formalism, *J. Phys. A: Math. Theor.* **43**, 103001 (2010).
- [59] C. Karrasch, *The functional renormalization group for zero-dimensional quantum systems in and out of equilibrium*, Ph.D. thesis, RWTH Aachen University, Germany, Aachen (2010), aachen, Techn. Hochsch., Diss., 2010.
- [60] C. Karrasch, *Transport Through Correlated Quantum Dots – A Functional Renormalization Group Approach* (2006), [arXiv:cond-mat/0612329 \[cond-mat.str-el\]](https://arxiv.org/abs/cond-mat/0612329).
- [61] A. A. Katanin, Fulfillment of Ward identities in the functional renormalization group approach, *Phys. Rev. B* **70**, 115109 (2004).
- [62] J. W. Negele, *Quantum many-particle systems* (CRC Press, 2018).
- [63] M. L. Baez, *Numerical methods for frustrated magnetism*, *Dissertation*, Freie Universität Berlin (2018).
- [64] F. L. Büßen, *A Functional Renormalization Group Perspective on Quantum Spin Liquids in Three-Dimensional Frustrated Magnets*, Ph.D. thesis, Universität zu Köln (2019).
- [65] K. Millard and H. S. Leff, Infinite-Spin Limit of the Quantum Heisenberg Model, *J. Math. Phys.* **12**, 1000 (1971).
- [66] E. H. Lieb, The classical limit of quantum spin systems, *Commun. Math. Phys.* **31**, 327 (1973).
- [67] If we stayed in the \pm basis, the generalized FDT's would be easy to implement but the causality relations then are difficult. We decided to use the Keldysh basis, since the FDT's are only fulfilled in equilibrium and thus not as general as the causality relations.
- [68] V. Nocolak and J. Reuther, Pseudo-fermion functional renormalization group with magnetic fields, *Phys. Rev. B* **109**, 174414 (2024).
- [69] F. Bippus, B. Schneider, and B. Sbierski, Pseudo-Majorana functional renormalization for frustrated XXZ spin- $\frac{1}{2}$ models with field or magnetization along the spin- Z direction at finite temperature, *Phys. Rev. B* **111**, 054420 (2025).
- [70] D. Kiese, T. Müller, Y. Iqbal, R. Thomale, and S. Trebst, Multiloop functional renormalization group approach to quantum spin systems, *Phys. Rev. Res.* **4**, 023185 (2022).
- [71] M. K. Ritter, D. Kiese, T. Müller, F. B. Kugler, R. Thomale, S. Trebst, and J. von Delft, Benchmark calculations of multi-loop pseudofermion fRG, *Eur. Phys. J. B* **95**, 102 (2022).
- [72] Note, that this choice of lattice cutoff is not possible for direct RPA calculations, where the inversion in Eq. (29) is only possible for a finite lattice.
- [73] N. Wentzell, G. Li, A. Tagliavini, C. Taranto, G. Rohringer, K. Held, A. Toschi, and S. Andergassen, High-frequency asymptotics of the vertex function: Diagrammatic parametrization and algorithmic implementation, *Phys. Rev. B* **102**, 085106 (2020).
- [74] E. Hairer, S. P. Nørsett, and G. Wanner, *Solving Ordinary Differential Equations I* (Springer Berlin, Heidelberg, 1993).
- [75] J. Beyer, F. Goth, and T. Müller, Better integrators for functional renormalization group calculations, *Eur. Phys. J. B* **95**, 116 (2022).
- [76] E. T. Whittaker and G. Robinson, *The calculus of observations: An introduction to numerical analysis* (Dover Publications, 1967).
- [77] L. F. Richardson and R. T. Glazebrook, IX. The approximate arithmetical solution by finite differences of physical problems involving differential equations, with an application to the stresses in a masonry dam, *Philos. Trans. R. Soc. A* **210**, 307 (1911).
- [78] N. Niggemann, Y. Iqbal, and J. Reuther, Quantum Effects on Unconventional Pinch Point Singularities, *Phys. Rev. Lett.* **130**, 196601 (2023).
- [79] V. Nocolak, D. Lozano-Gómez, J. Oitmaa, R. R. P. Singh, Y. Iqbal, M. J. P. Gingras, and J. Reuther, Classical and quantum phases of the pyrochlore $S = \frac{1}{2}$ magnet with Heisenberg and Dzyaloshinskii-Moriya interactions, *Phys. Rev. B* **107**, 214414 (2023).
- [80] D. Lozano-Gómez, V. Nocolak, J. Oitmaa, R. R. P. Singh, Y. Iqbal, J. Reuther, and M. J. P. Gingras, Competing gauge fields and entropically driven spin liquid to spin liquid transition in non-Kramers pyrochlores, *Proc. Natl. Acad. Sci. U.S.A.* **121**, e2403487121 (2024).
- [81] L. Gresista, D. Lozano-Gómez, M. Vojta, S. Trebst, and Y. Iqbal, *Quantum effects on pyrochlore higher-rank U(1) spin liquids: pinch-line singularities, spin nematics, and connections to oxide materials* (2025), [arXiv:2503.03749 \[cond-mat.str-el\]](https://arxiv.org/abs/2503.03749).
- [82] P. Ghosh, Y. Iqbal, T. Müller, R. T. Ponnaganti, R. Thomale, R. Narayanan, J. Reuther, M. J. P. Gingras, and H. O. Jeschke, Breathing chromium spinels: a showcase for a variety of pyrochlore Heisenberg Hamiltonians, *npj Quantum Mater.* **4**, 63 (2019).
- [83] P. Ghosh, T. Müller, F. P. Toldin, J. Richter, R. Narayanan, R. Thomale, J. Reuther, and Y. Iqbal, Quantum paramagnetism and helimagnetic orders in the Heisenberg model on the body centered cubic lattice, *Phys. Rev. B* **100**, 014420 (2019).
- [84] Y. Iqbal, T. Müller, P. Ghosh, M. J. P. Gingras, H. O. Jeschke, S. Rachel, J. Reuther, and R. Thomale, Quantum and Classical Phases of the Pyrochlore Heisenberg Model with Competing Interactions, *Phys. Rev. X* **9**, 011005 (2019).
- [85] Y. Iqbal, T. Müller, H. O. Jeschke, R. Thomale, and J. Reuther, Stability of the spiral spin liquid in MnSc_2S_4 , *Phys. Rev. B* **98**, 064427 (2018).
- [86] Y. Iqbal, T. Müller, K. Riedl, J. Reuther, S. Rachel, R. Valentí, M. J. P. Gingras, R. Thomale, and H. O. Jeschke, Signatures of a gearwheel quantum spin liquid in a spin- $\frac{1}{2}$ pyrochlore molybdate Heisenberg antiferromagnet, *Phys. Rev. Mater.* **1**, 071201 (2017).
- [87] Y. Iqbal, R. Thomale, F. Parisen Toldin, S. Rachel, and J. Reuther, Functional renormalization group for three-dimensional quantum magnetism, *Phys. Rev. B* **94**, 140408 (2016).

- [88] F. Bloch, Zur Theorie des Ferromagnetismus, *Z. Physik* **61**, 206 (1930).
- [89] S. Toth and B. Lake, Linear spin wave theory for single-Q incommensurate magnetic structures, *J. Phys. Condens. Matter* **27**, 166002 (2015).
- [90] T. Müller, *Quantum magnetism in three dimensions - Exploring phase diagrams and real materials using Functional Renormalization*, Ph.D. thesis, Julius-Maximilians Universität Würzburg (2022).
- [91] F. Ferrari and F. Becca, Spectral signatures of fractionalization in the frustrated Heisenberg model on the square lattice, *Phys. Rev. B* **98**, 100405 (2018).
- [92] F. D. M. Haldane, “fractional statistics” in arbitrary dimensions: A generalization of the pauli principle, *Phys. Rev. Lett.* **67**, 937 (1991).
- [93] S. R. White and I. Affleck, Dimerization and incommensurate spiral spin correlations in the zigzag spin chain: Analogies to the Kondo lattice, *Phys. Rev. B* **54**, 9862 (1996).
- [94] H. Bethe, Zur Theorie der Metalle: I. Eigenwerte und Eigenfunktionen der linearen Atomkette, *Z. Physik* **71**, 205 (1931).
- [95] S. R. White and I. Affleck, Dimerization and incommensurate spiral spin correlations in the zigzag spin chain: Analogies to the Kondo lattice, *Phys. Rev. B* **54**, 9862 (1996).
- [96] C. K. Majumdar and D. K. Ghosh, On Next-Nearest-Neighbor Interaction in Linear Chain. I, *J. Math. Phys.* **10**, 1388 (1969).
- [97] F. Ferrari, A. Parola, S. Sorella, and F. Becca, Dynamical structure factor of the $J_1 - J_2$ Heisenberg model in one dimension: The variational Monte Carlo approach, *Phys. Rev. B* **97**, 235103 (2018).
- [98] O. Starykh, A. Sandvik, and R. Singh, Finite temperature dynamics of the spin-half Heisenberg chain, *Phys. B: Condens. Matter* **241-243**, 563 (1997), proceedings of the International Conference on Neutron Scattering.
- [99] D. A. Tennant, R. A. Cowley, S. E. Nagler, and A. M. Tsvelik, Measurement of the spin-excitation continuum in one-dimensional KCuF_3 using neutron scattering, *Phys. Rev. B* **52**, 13368 (1995).
- [100] T. Müller, D. Kiese, and L. Gresista, `dominikkiese/PFFRGSolver.jl: v0.5.1` (2023).
- [101] J. Knolle, D. L. Kovrizhin, J. T. Chalker, and R. Moessner, Dynamics of fractionalization in quantum spin liquids, *Phys. Rev. B* **92**, 115127 (2015).
- [102] J.-i. Igarashi and T. Nagao, $1/S$ -expansion study of spin waves in a two-dimensional Heisenberg antiferromagnet, *Phys. Rev. B* **72**, 014403 (2005).
- [103] N. B. Christensen, H. M. Rønnow, D. F. McMorrow, A. Harrison, T. G. Perring, M. Enderle, R. Coldea, L. P. Regnault, and G. Aeppli, Quantum dynamics and entanglement of spins on a square lattice, *Proc. Natl. Acad. Sci. U.S.A* **104**, 15264 (2007).
- [104] R. R. P. Singh, Thermodynamic parameters of the $T = 0$, spin-1/2 square-lattice Heisenberg antiferromagnet, *Phys. Rev. B* **39**, 9760 (1989).
- [105] R. R. P. Singh and M. P. Gelfand, Spin-wave excitation spectra and spectral weights in square lattice antiferromagnets, *Phys. Rev. B* **52**, R15695 (1995).
- [106] A. W. Sandvik and R. R. P. Singh, High-Energy Magnon Dispersion and Multimagnon Continuum in the Two-Dimensional Heisenberg Antiferromagnet, *Phys. Rev. Lett.* **86**, 528 (2001).
- [107] B. Dalla Piazza, M. Mourigal, N. B. Christensen, G. J. Nilsen, P. Tregenna-Piggott, T. G. Perring, M. Enderle, D. F. McMorrow, D. A. Ivanov, and H. M. Rønnow, Fractional excitations in the square-lattice quantum antiferromagnet, *Nat. Phys.* **11**, 62 (2015).
- [108] H. Shao, Y. Q. Qin, S. Capponi, S. Chesi, Z. Y. Meng, and A. W. Sandvik, Nearly Deconfined Spinon Excitations in the Square-Lattice Spin-1/2 Heisenberg Antiferromagnet, *Phys. Rev. X* **7**, 041072 (2017).
- [109] S.-L. Yu, W. Wang, Z.-Y. Dong, Z.-J. Yao, and J.-X. Li, Deconfinement of spinons in frustrated spin systems: Spectral perspective, *Phys. Rev. B* **98**, 134410 (2018).
- [110] W.-J. Hu, F. Becca, A. Parola, and S. Sorella, Direct evidence for a gapless Z_2 spin liquid by frustrating Néel antiferromagnetism, *Phys. Rev. B* **88**, 060402 (2013).
- [111] C. Taranto, S. Andergassen, J. Bauer, K. Held, A. Katanin, W. Metzner, G. Rohringer, and A. Toschi, From Infinite to Two Dimensions through the Functional Renormalization Group, *Phys. Rev. Lett.* **112**, 196402 (2014).
- [112] J. Knolle, D. L. Kovrizhin, J. T. Chalker, and R. Moessner, Dynamics of a Two-Dimensional Quantum Spin Liquid: Signatures of Emergent Majorana Fermions and Fluxes, *Phys. Rev. Lett.* **112**, 207203 (2014).
- [113] H. Takagi, T. Takayama, G. Jackeli, G. Khaliullin, and S. E. Nagler, Concept and realization of kitaev quantum spin liquids, *Nat. Rev. Phys.* **1**, 264 (2019).
- [114] R. Gezzi, T. Pruschke, and V. Meden, Functional renormalization group for nonequilibrium quantum many-body problems, *Phys. Rev. B* **75**, 045324 (2007).

Appendix A: Full FRG Flow equations

In this section we present the flow equations for the Kitaev model, which can be easily simplified into the pure $SU(2)$ symmetric Heisenberg model by $\Gamma_{xx} = \Gamma_{yy} = \Gamma_{zz} = \Gamma_s$. The flow equations are obtained by inserting the vertex decomposition Eq. (23) into the flow Eq. (18). After performing all spin sums we arrive at the full flow equations.

$$\begin{aligned}
\frac{d}{d\Lambda} \Gamma_{xx i_1 i_2}^{\Lambda 1'2'|12}(1', 2'|1, 2) &= \frac{1}{2\pi} \sum_{\alpha_3 \alpha_3'} \sum_{\alpha_4 \alpha_4'} \int d\omega_3 \int d\omega_4 \left(G_{\alpha_3 \alpha_3'}^{\Lambda}(\omega_3) S_{\alpha_4 \alpha_4'}^{\Lambda}(\omega_4) + G_{\alpha_4 \alpha_4'}^{\Lambda}(\omega_4) S_{\alpha_3 \alpha_3'}^{\Lambda}(\omega_3) \right) \\
&\left\{ \left[\Gamma_{xx i_1 i_2}^{\Lambda 1'2'|34}(1', 2'|3, 4) \Gamma_{d i_1 i_2}^{\Lambda 3'4'|12}(3, 4|1, 2) - \Gamma_{yy i_1 i_2}^{\Lambda 1'2'|34}(1', 2'|3, 4) \Gamma_{zz i_1 i_2}^{\Lambda 3'4'|12}(3, 4|1, 2) \right. \right. \\
&\quad \left. \left. - \Gamma_{zz i_1 i_2}^{\Lambda 1'2'|34}(1', 2'|3, 4) \Gamma_{yy i_1 i_2}^{\Lambda 3'4'|12}(3, 4|1, 2) + \Gamma_{d i_1 i_2}^{\Lambda 1'2'|34}(1', 2'|3, 4) \Gamma_{xx i_1 i_2}^{\Lambda 3'4'|12}(3, 4|1, 2) \right] \right. \\
&\quad \times \delta(\omega_3 + \omega_4 - \omega_{1'} - \omega_{2'}) \delta(\omega_1 + \omega_2 - \omega_3 - \omega_4) \\
&- 2 \sum_{i_3} \Gamma_{xx i_1 i_3}^{\Lambda 1'4'|13}(1', 4|1, 3) \Gamma_{xx i_3 i_1}^{\Lambda 3'2'|42}(3, 2'|4, 2) \delta(\omega_1 + \omega_3 - \omega_{1'} - \omega_4) \delta(\omega_4 + \omega_2 - \omega_3 - \omega_2) \\
&\quad + \left[\Gamma_{xx i_1 i_2}^{\Lambda 1'4'|13}(1', 4|1, 3) \Gamma_{xx i_2 i_2}^{\Lambda 3'2'|24}(3, 2'|2, 4) - \Gamma_{xx i_1 i_2}^{\Lambda 1'4'|13}(1', 4|1, 3) \Gamma_{yy i_2 i_2}^{\Lambda 3'2'|24}(3, 2'|2, 4) \right. \\
&\quad \left. - \Gamma_{xx i_1 i_2}^{\Lambda 1'4'|13}(1', 4|1, 3) \Gamma_{zz i_2 i_2}^{\Lambda 3'2'|24}(3, 2'|2, 4) + \Gamma_{xx i_1 i_2}^{\Lambda 1'4'|13}(1', 4|1, 3) \Gamma_{d i_2 i_2}^{\Lambda 3'2'|24}(3, 2'|2, 4) \right] \\
&\quad \times \delta(\omega_1 + \omega_3 - \omega_{1'} - \omega_4) \delta(\omega_2 + \omega_4 - \omega_3 - \omega_{2'}) \\
&\quad + \left[\Gamma_{xx i_1 i_1}^{\Lambda 1'4'|31}(1', 4|3, 1) \Gamma_{xx i_1 i_2}^{\Lambda 3'2'|42}(3, 2'|4, 2) - \Gamma_{yy i_1 i_1}^{\Lambda 1'4'|31}(1', 4|3, 1) \Gamma_{xx i_1 i_2}^{\Lambda 3'2'|42}(3, 2'|4, 2) \right. \\
&\quad \left. - \Gamma_{zz i_1 i_1}^{\Lambda 1'4'|31}(1', 4|3, 1) \Gamma_{xx i_1 i_2}^{\Lambda 3'2'|42}(3, 2'|4, 2) + \Gamma_{d i_1 i_1}^{\Lambda 1'4'|31}(1', 4|3, 1) \Gamma_{xx i_1 i_2}^{\Lambda 3'2'|42}(3, 2'|4, 2) \right] \\
&\quad \times \delta(\omega_3 + \omega_1 - \omega_{1'} - \omega_4) \delta(\omega_4 + \omega_2 - \omega_3 - \omega_{2'}) \\
&\quad + \left[\Gamma_{xx i_1 i_2}^{\Lambda 3'2'|14}(3, 2'|1, 4) \Gamma_{d i_1 i_2}^{\Lambda 1'4'|32}(1', 4|3, 2) + \Gamma_{yy i_1 i_2}^{\Lambda 3'2'|14}(3, 2'|1, 4) \Gamma_{zz i_1 i_2}^{\Lambda 1'4'|32}(1', 4|3, 2) \right. \\
&\quad \left. + \Gamma_{zz i_1 i_2}^{\Lambda 3'2'|14}(3, 2'|1, 4) \Gamma_{yy i_1 i_2}^{\Lambda 1'4'|32}(1', 4|3, 2) + \Gamma_{d i_1 i_2}^{\Lambda 3'2'|14}(3, 2'|1, 4) \Gamma_{xx i_1 i_2}^{\Lambda 1'4'|32}(1', 4|3, 2) \right] \\
&\quad \left. \times \delta(\omega_1 + \omega_4 - \omega_3 - \omega_{2'}) \delta(\omega_3 + \omega_2 - \omega_{1'} - \omega_4) \right\} \tag{A1}
\end{aligned}$$

$$\begin{aligned}
\frac{d}{d\Lambda} \Gamma_{yy i_1 i_2}^{\Lambda 1'2'|12}(1', 2'|1, 2) &= \frac{1}{2\pi} \sum_{\alpha_3 \alpha_3'} \sum_{\alpha_4 \alpha_4'} \int d\omega_3 \int d\omega_4 \left(G_{\alpha_3 \alpha_3'}^{\Lambda}(\omega_3) S_{\alpha_4 \alpha_4'}^{\Lambda}(\omega_4) + G_{\alpha_4 \alpha_4'}^{\Lambda}(\omega_4) S_{\alpha_3 \alpha_3'}^{\Lambda}(\omega_3) \right) \\
&\left\{ \begin{aligned}
&[-\Gamma_{xx i_1 i_2}^{\Lambda 1'2'|34}(1', 2'|3, 4) \Gamma_{zz i_1 i_2}^{\Lambda 3'4'|12}(3, 4|1, 2) + \Gamma_{yy i_1 i_2}^{\Lambda 1'2'|34}(1', 2'|3, 4) \Gamma_{d i_1 i_2}^{\Lambda 3'4'|12}(3, 4|1, 2) \\
&\quad - \Gamma_{zz i_1 i_2}^{\Lambda 1'2'|34}(1', 2'|3, 4) \Gamma_{xx i_1 i_2}^{\Lambda 3'4'|12}(3, 4|1, 2) + \Gamma_{d i_1 i_2}^{\Lambda 1'2'|34}(1', 2'|3, 4) \Gamma_{yy i_1 i_2}^{\Lambda 3'4'|12}(3, 4|1, 2)] \\
&\quad \times \delta(\omega_3 + \omega_4 - \omega_{1'} - \omega_{2'}) \delta(\omega_1 + \omega_2 - \omega_3 - \omega_4) \\
&- 2 \sum_{i_3} \Gamma_{yy i_1 i_3}^{\Lambda 1'4'|13}(1', 4|1, 3) \Gamma_{yy i_3 i_1}^{\Lambda 3'2'|42}(3, 2'|4, 2) \delta(\omega_1 + \omega_3 - \omega_{1'} - \omega_4) \delta(\omega_4 + \omega_2 - \omega_3 - \omega_2) \\
&\quad + [-\Gamma_{yy i_1 i_2}^{\Lambda 1'4'|13}(1', 4|1, 3) \Gamma_{xx i_2 i_2}^{\Lambda 3'2'|24}(3, 2'|2, 4) + \Gamma_{yy i_1 i_2}^{\Lambda 1'4'|13}(1', 4|1, 3) \Gamma_{yy i_2 i_2}^{\Lambda 3'2'|24}(3, 2'|2, 4) \\
&\quad - \Gamma_{yy i_1 i_2}^{\Lambda 1'4'|13}(1', 4|1, 3) \Gamma_{zz i_2 i_2}^{\Lambda 3'2'|24}(3, 2'|2, 4) + \Gamma_{yy i_1 i_2}^{\Lambda 1'4'|13}(1', 4|1, 3) \Gamma_{d i_2 i_2}^{\Lambda 3'2'|24}(3, 2'|2, 4)] \\
&\quad \times \delta(\omega_1 + \omega_3 - \omega_{1'} - \omega_4) \delta(\omega_2 + \omega_4 - \omega_3 - \omega_{2'}) \\
&\quad + [-\Gamma_{xx i_1 i_1}^{\Lambda 1'4'|31}(1', 4|3, 1) \Gamma_{yy i_1 i_2}^{\Lambda 3'2'|42}(3, 2'|4, 2) + \Gamma_{yy i_1 i_1}^{\Lambda 1'4'|31}(1', 4|3, 1) \Gamma_{yy i_1 i_2}^{\Lambda 3'2'|42}(3, 2'|4, 2) \\
&\quad - \Gamma_{zz i_1 i_1}^{\Lambda 1'4'|31}(1', 4|3, 1) \Gamma_{yy i_1 i_2}^{\Lambda 3'2'|42}(3, 2'|4, 2) + \Gamma_{d i_1 i_1}^{\Lambda 1'4'|31}(1', 4|3, 1) \Gamma_{yy i_1 i_2}^{\Lambda 3'2'|42}(3, 2'|4, 2)] \\
&\quad \times \delta(\omega_3 + \omega_1 - \omega_{1'} - \omega_4) \delta(\omega_4 + \omega_2 - \omega_3 - \omega_{2'}) \\
&\quad + [\Gamma_{xx i_1 i_2}^{\Lambda 3'2'|14}(3, 2'|1, 4) \Gamma_{zz i_1 i_2}^{\Lambda 1'4'|32}(1', 4|3, 2) + \Gamma_{yy i_1 i_2}^{\Lambda 3'2'|14}(3, 2'|1, 4) \Gamma_{d i_1 i_2}^{\Lambda 1'4'|32}(1', 4|3, 2) \\
&\quad + \Gamma_{zz i_1 i_2}^{\Lambda 3'2'|14}(3, 2'|1, 4) \Gamma_{xx i_1 i_2}^{\Lambda 1'4'|32}(1', 4|3, 2) + \Gamma_{d i_1 i_2}^{\Lambda 3'2'|14}(3, 2'|1, 4) \Gamma_{yy i_1 i_2}^{\Lambda 1'4'|32}(1', 4|3, 2)] \\
&\quad \times \delta(\omega_1 + \omega_4 - \omega_3 - \omega_{2'}) \delta(\omega_3 + \omega_2 - \omega_{1'} - \omega_4) \left. \vphantom{\int} \right\} \tag{A2}
\end{aligned}
\right.
\end{aligned}$$

$$\begin{aligned}
\frac{d}{d\Lambda} \Gamma_{zz i_1 i_2}^{\Lambda 1'2'|12}(1', 2'|1, 2) &= \frac{1}{2\pi} \sum_{\alpha_3 \alpha_3'} \sum_{\alpha_4 \alpha_4'} \int d\omega_3 \int d\omega_4 \left(G_{\alpha_3 \alpha_3'}^{\Lambda}(\omega_3) S_{\alpha_4 \alpha_4'}^{\Lambda}(\omega_4) + G_{\alpha_4 \alpha_4'}^{\Lambda}(\omega_4) S_{\alpha_3 \alpha_3'}^{\Lambda}(\omega_3) \right) \\
&\left\{ \begin{aligned}
&[-\Gamma_{xx i_1 i_2}^{\Lambda 1'2'|34}(1', 2'|3, 4) \Gamma_{yy i_1 i_2}^{\Lambda 3'4'|12}(3, 4|1, 2) - \Gamma_{yy i_1 i_2}^{\Lambda 1'2'|34}(1', 2'|3, 4) \Gamma_{xx i_1 i_2}^{\Lambda 3'4'|12}(3, 4|1, 2) \\
&\quad + \Gamma_{zz i_1 i_2}^{\Lambda 1'2'|34}(1', 2'|3, 4) \Gamma_{d i_1 i_2}^{\Lambda 3'4'|12}(3, 4|1, 2) + \Gamma_{d i_1 i_2}^{\Lambda 1'2'|34}(1', 2'|3, 4) \Gamma_{zz i_1 i_2}^{\Lambda 3'4'|12}(3, 4|1, 2)] \\
&\quad \times \delta(\omega_3 + \omega_4 - \omega_{1'} - \omega_{2'}) \delta(\omega_1 + \omega_2 - \omega_3 - \omega_4) \\
&- 2 \sum_{i_3} \Gamma_{zz i_1 i_3}^{\Lambda 1'4'|13}(1', 4|1, 3) \Gamma_{zz i_3 i_1}^{\Lambda 3'2'|42}(3, 2'|4, 2) \delta(\omega_1 + \omega_3 - \omega_{1'} - \omega_4) \delta(\omega_4 + \omega_2 - \omega_3 - \omega_2) \\
&\quad + [-\Gamma_{zz i_1 i_2}^{\Lambda 1'4'|13}(1', 4|1, 3) \Gamma_{xx i_2 i_2}^{\Lambda 3'2'|24}(3, 2'|2, 4) - \Gamma_{zz i_1 i_2}^{\Lambda 1'4'|13}(1', 4|1, 3) \Gamma_{yy i_2 i_2}^{\Lambda 3'2'|24}(3, 2'|2, 4) \\
&\quad + \Gamma_{zz i_1 i_2}^{\Lambda 1'4'|13}(1', 4|1, 3) \Gamma_{zz i_2 i_2}^{\Lambda 3'2'|24}(3, 2'|2, 4) + \Gamma_{zz i_1 i_2}^{\Lambda 1'4'|13}(1', 4|1, 3) \Gamma_{d i_2 i_2}^{\Lambda 3'2'|24}(3, 2'|2, 4)] \\
&\quad \times \delta(\omega_1 + \omega_3 - \omega_{1'} - \omega_4) \delta(\omega_2 + \omega_4 - \omega_3 - \omega_{2'}) \\
&\quad + [-\Gamma_{xx i_1 i_1}^{\Lambda 1'4'|31}(1', 4|3, 1) \Gamma_{zz i_1 i_2}^{\Lambda 3'2'|42}(3, 2'|4, 2) - \Gamma_{yy i_1 i_1}^{\Lambda 1'4'|31}(1', 4|3, 1) \Gamma_{zz i_1 i_2}^{\Lambda 3'2'|42}(3, 2'|4, 2) \\
&\quad + \Gamma_{zz i_1 i_1}^{\Lambda 1'4'|31}(1', 4|3, 1) \Gamma_{zz i_1 i_2}^{\Lambda 3'2'|42}(3, 2'|4, 2) + \Gamma_{d i_1 i_1}^{\Lambda 1'4'|31}(1', 4|3, 1) \Gamma_{zz i_1 i_2}^{\Lambda 3'2'|42}(3, 2'|4, 2)] \\
&\quad \times \delta(\omega_3 + \omega_1 - \omega_{1'} - \omega_4) \delta(\omega_4 + \omega_2 - \omega_3 - \omega_{2'}) \\
&\quad + [\Gamma_{xx i_1 i_2}^{\Lambda 3'2'|14}(3, 2'|1, 4) \Gamma_{yy i_1 i_2}^{\Lambda 1'4'|32}(1', 4|3, 2) + \Gamma_{yy i_1 i_2}^{\Lambda 3'2'|14}(3, 2'|1, 4) \Gamma_{xx i_1 i_2}^{\Lambda 1'4'|32}(1', 4|3, 2) \\
&\quad + \Gamma_{zz i_1 i_2}^{\Lambda 3'2'|14}(3, 2'|1, 4) \Gamma_{d i_1 i_2}^{\Lambda 1'4'|32}(1', 4|3, 2) + \Gamma_{d i_1 i_2}^{\Lambda 3'2'|14}(3, 2'|1, 4) \Gamma_{zz i_1 i_2}^{\Lambda 1'4'|32}(1', 4|3, 2)] \\
&\quad \times \delta(\omega_1 + \omega_4 - \omega_3 - \omega_{2'}) \delta(\omega_3 + \omega_2 - \omega_{1'} - \omega_4) \left. \vphantom{\int} \right\} \tag{A3}
\end{aligned}
\right.
\end{aligned}$$

$$\begin{aligned}
\frac{d}{d\Lambda} \Gamma_{d i_1 i_2}^{\Lambda 1'2'|12}(1', 2'|1, 2) &= \frac{1}{2\pi} \sum_{\alpha_3 \alpha_3'} \sum_{\alpha_4 \alpha_4'} \int d\omega_3 \int d\omega_4 \left(G_{\alpha_3 \alpha_3'}^{\Lambda}(\omega_3) S_{\alpha_4 \alpha_4'}^{\Lambda}(\omega_4) + G_{\alpha_4 \alpha_4'}^{\Lambda}(\omega_4) S_{\alpha_3 \alpha_3'}^{\Lambda}(\omega_3) \right) \\
&\left\{ \left[\Gamma_{xx i_1 i_2}^{\Lambda 1'2'|34}(1', 2'|3, 4) \Gamma_{xx i_1 i_2}^{\Lambda 3'4'|12}(3, 4|1, 2) + \Gamma_{yy i_1 i_2}^{\Lambda 1'2'|34}(1', 2'|3, 4) \Gamma_{yy i_1 i_2}^{\Lambda 3'4'|12}(3, 4|1, 2) \right. \right. \\
&\quad \left. \left. + \Gamma_{zz i_1 i_2}^{\Lambda 1'2'|34}(1', 2'|3, 4) \Gamma_{zz i_1 i_2}^{\Lambda 3'4'|12}(3, 4|1, 2) + \Gamma_{d i_1 i_2}^{\Lambda 1'2'|34}(1', 2'|3, 4) \Gamma_{d i_1 i_2}^{\Lambda 3'4'|12}(3, 4|1, 2) \right] \right. \\
&\quad \times \delta(\omega_3 + \omega_4 - \omega_{1'} - \omega_{2'}) \delta(\omega_1 + \omega_2 - \omega_3 - \omega_4) \\
&- 2 \sum_{i_3} \Gamma_{d i_1 i_3}^{\Lambda 1'4'|13}(1', 4|1, 3) \Gamma_{d i_3 i_1}^{\Lambda 3'2'|42}(3, 2'|4, 2) \delta(\omega_1 + \omega_3 - \omega_{1'} - \omega_4) \delta(\omega_4 + \omega_2 - \omega_3 - \omega_2) \\
&\quad \left[\Gamma_{d i_1 i_2}^{\Lambda 1'4'|13}(1', 4|1, 3) \Gamma_{xx i_2 i_2}^{\Lambda 3'2'|24}(3, 2'|2, 4) + \Gamma_{d i_1 i_2}^{\Lambda 1'4'|13}(1', 4|1, 3) \Gamma_{yy i_2 i_2}^{\Lambda 3'2'|24}(3, 2'|2, 4) \right. \\
&\quad \left. + \Gamma_{d i_1 i_2}^{\Lambda 1'4'|13}(1', 4|1, 3) \Gamma_{zz i_2 i_2}^{\Lambda 3'2'|24}(3, 2'|2, 4) + \Gamma_{d i_1 i_2}^{\Lambda 1'4'|13}(1', 4|1, 3) \Gamma_{d i_2 i_2}^{\Lambda 3'2'|24}(3, 2'|2, 4) \right] \\
&\quad \times \delta(\omega_1 + \omega_3 - \omega_{1'} - \omega_4) \delta(\omega_2 + \omega_4 - \omega_3 - \omega_{2'}) \\
&+ \left[\Gamma_{xx i_1 i_1}^{\Lambda 1'4'|31}(1', 4|3, 1) \Gamma_{d i_1 i_2}^{\Lambda 3'2'|42}(3, 2'|4, 2) + \Gamma_{yy i_1 i_1}^{\Lambda 1'4'|31}(1', 4|3, 1) \Gamma_{d i_1 i_2}^{\Lambda 3'2'|42}(3, 2'|4, 2) \right. \\
&\quad \left. + \Gamma_{zz i_1 i_1}^{\Lambda 1'4'|31}(1', 4|3, 1) \Gamma_{d i_1 i_2}^{\Lambda 3'2'|42}(3, 2'|4, 2) + \Gamma_{d i_1 i_1}^{\Lambda 1'4'|31}(1', 4|3, 1) \Gamma_{d i_1 i_2}^{\Lambda 3'2'|42}(3, 2'|4, 2) \right] \\
&\quad \times \delta(\omega_3 + \omega_1 - \omega_{1'} - \omega_4) \delta(\omega_4 + \omega_2 - \omega_3 - \omega_{2'}) \\
&+ \left[\Gamma_{xx i_1 i_2}^{\Lambda 3'2'|14}(3, 2'|1, 4) \Gamma_{xx i_1 i_2}^{\Lambda 1'4'|32}(1', 4|3, 2) + \Gamma_{yy i_1 i_2}^{\Lambda 3'2'|14}(3, 2'|1, 4) \Gamma_{yy i_1 i_2}^{\Lambda 1'4'|32}(1', 4|3, 2) \right. \\
&\quad \left. + \Gamma_{zz i_1 i_2}^{\Lambda 3'2'|14}(3, 2'|1, 4) \Gamma_{zz i_1 i_2}^{\Lambda 1'4'|32}(1', 4|3, 2) + \Gamma_{d i_1 i_2}^{\Lambda 3'2'|14}(3, 2'|1, 4) \Gamma_{d i_1 i_2}^{\Lambda 1'4'|32}(1', 4|3, 2) \right] \\
&\quad \left. \times \delta(\omega_1 + \omega_4 - \omega_3 - \omega_{2'}) \delta(\omega_3 + \omega_2 - \omega_{1'} - \omega_4) \right\} \tag{A4}
\end{aligned}$$

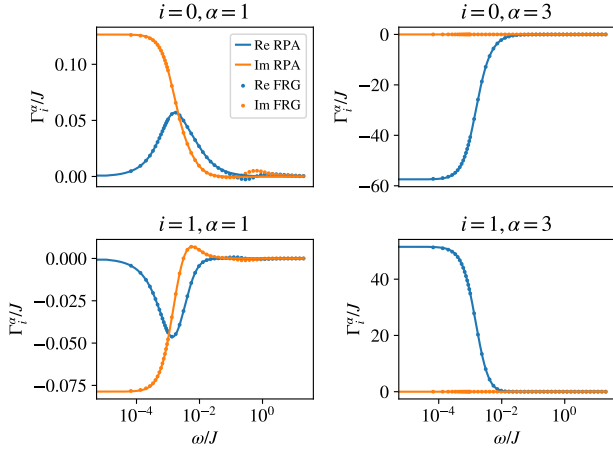


Figure 9. Independent vertex components in the large S -limit at $\Lambda = 0.002J \ll T = 0.2J$. The FRG data results from a single channel FRG flow with $N_{\text{FRG}} = 50$ while the RPA data is computed in a single step for the given cutoff with a higher resolution of $N_{\text{RPA}} = 300$. The results are nearly identical on vertex level and only a remeshing artifact around $\omega = J$ is visible for the FRG data.

Appendix B: Vertex comparison RPA - FRG

To show the equivalence of the FRG and the RPA results we show the comparison of the results on vertex level. In the single-channel flow we only get two independent Keldysh indices, which can be chosen to be e.g. $(0, 0, 0, 1) \leftrightarrow \alpha = 1$ and $(0, 0, 1, 1) \leftrightarrow \alpha = 3$. All other components can be related to these by symmetry operations as e.g. complex conjugation ($1 \leftrightarrow 2$). We show these independent components $\alpha = 1, 3$ in Fig. 9. There one can see, that the FRG results with $N_{\text{FRG}} = 50$ are nearly identical to the RPA results with a much higher resolution of $N_{\text{RPA}} = 300$. The resolution for the FRG was chosen to be similar to the FRG flows which were performed for the full Heisenberg model to highlight potential difficulties of the FRG. The notable difference between the FRG and RPA results is a wiggle around $\omega = 1$ for all independent vertices, albeit being most noticeable for $i = 0, \alpha = 1$. This is a result of the remeshing procedure, as we refine our frequency mesh during the flow to accurately capture the essential features at each energy scale. This would have not been necessary for the RPA, as the RPA flow is independent for each frequency, thus allowing us to perform the RPA calculations for each frequency. However, this is not true for the full FRG. Nevertheless, these effects can be minimized by increasing the number of frequencies N_{FRG} or optimizing the mesh parameters and seem to play a minor role in the calculation of all our observables. Due to this, we can say, that the FRG accurately reproduces the single step RPA results, highlighting the robustness of the flow and the solving method for the differential equations.

Appendix C: Dimer results at lower temperature

At lower temperatures, the dimer exhibits a kink in the flow, which signals a divergence in the susceptibility and thus ordering tendencies. Since the FRG flow is only defined in the paramagnetic phase, the flow would need to be stopped at this point. The first time, a small increase after the saturation in the nearest neighbor correlator is observable is at $T = 0.1J$, albeit being almost non-detectable. This is shown in Fig. 10. There, we also show the flow at $T = 0.01J$, where the breakdown of the flow is visible much clearer. The breakdown of the flow is also further supported by the double Gaussian fit, as described in the main text (cf. Eq. (51)). The extracted broadenings – shown in Fig. 11 – which should be correlated to the temperature, feature a step around $T = 0.2$. This further indicates the onset of an ordered phase, where the FRG is not valid anymore. Apart from that, we also show the peak positions from the physical peak in Fig. 11, where one can see that the physical value of $\omega/J = 1$ is only crossed but the $T \rightarrow 0$ value does not saturate to. Instead, we see a monotonous increase when decreasing the temperature. This further highlights the findings in the main text, where we should not use the method below $T = 0.1J$.

Appendix D: Extended symmetry table

In the following we will highlight the symmetries of the self-energy Σ and the two particle vertex functions Γ . We will do so in the asymptotic parametrization [73], as it is used in the implementation. We use the following definition for the pre-factors

$$\zeta(\alpha) = (-1)^{\sum_i (\alpha'_i + \alpha_i)}, \quad (\text{D1})$$

$$\xi(\mu) = \begin{cases} +1 & \mu = 0 \\ -1 & \mu = x, y, z \end{cases}. \quad (\text{D2})$$

These pre-factors are a consequence of the symmetry under complex conjugation ($\zeta(\alpha)$) or due to the particle hole symmetries and a resulting reordering of the Pauli matrices ($\xi(\mu)$).

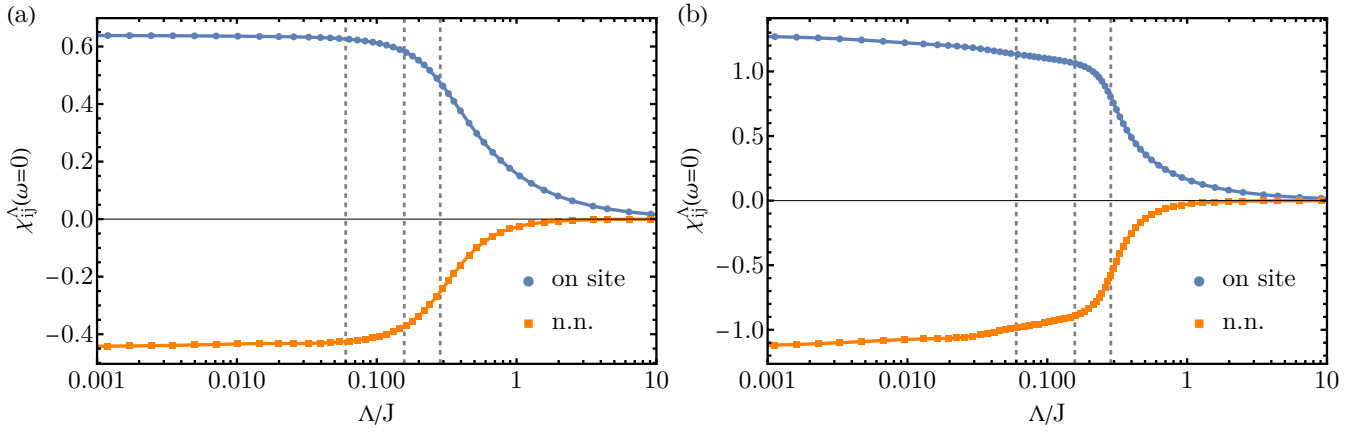


Figure 10. FRG Flow for the AFM Dimer at (a) $T = 0.1J$ and (b) $T = 0.01J$. The flow exhibits unphysical saturation points, which hint at a breakdown of the flow. Due to this, these results should only be trusted up to the cutoff of the divergence.

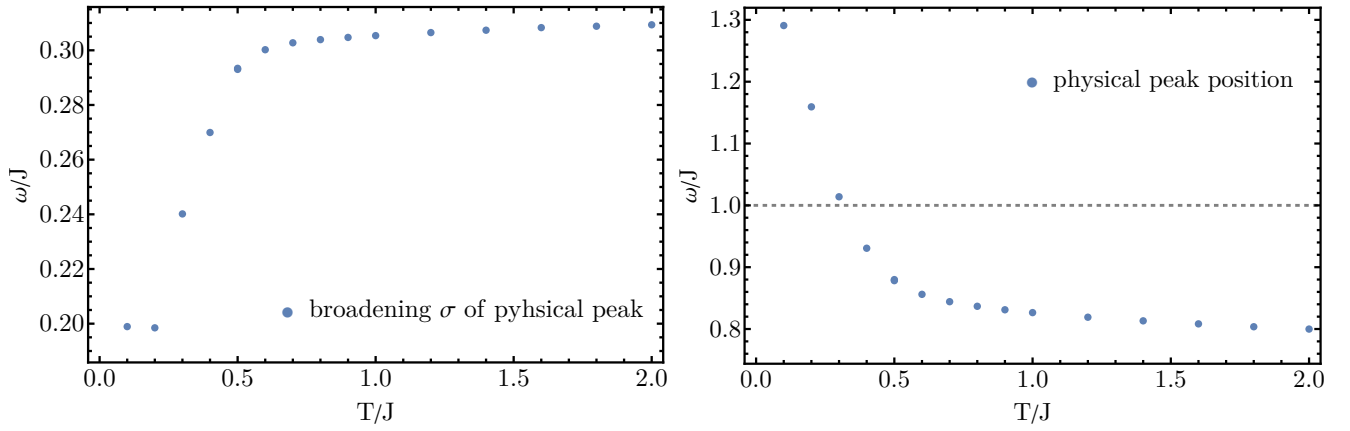


Figure 11. Fit parameters for the AFM dimers at different temperatures. Given are only the values of the physical peak. The peak position shifts with temperature, while the correct value of ω/J is only passed. The broadening of the peak seems to be fixed around $0.2J$, which could be due to the slight bump, which first emerges at $T = 0.1J$

$\Sigma^{\alpha'} \alpha(\omega) = -\zeta(\boldsymbol{\alpha})[\Sigma^{\alpha} \alpha'(\omega)]^*$	(CC)
$\Sigma^{\alpha'} \alpha(\omega) = -\Sigma^{\alpha} \alpha'(-\omega)$	(PH)
$\Gamma_{\mu\nu i_1 i_2}^{s, \alpha'_1 \alpha'_2} \alpha_1 \alpha_2(s, \nu_s, \nu'_s) = \zeta(\boldsymbol{\alpha})[\Gamma_{\nu\mu i_2 i_1}^{s, \alpha'_2 \alpha'_1} \alpha_2 \alpha_1(-s, \nu_s, \nu'_s)]^*$	(X \circ CC \circ PH1 \circ PH2)
$\Gamma_{\mu\nu i_1 i_2}^{s, \alpha'_1 \alpha'_2} \alpha_1 \alpha_2(s, \nu_s, \nu'_s) = -\xi(\mu) \Gamma_{\nu\mu i_2 i_1}^{u, \alpha'_2 \alpha_1} \alpha_2 \alpha'_1(s, -\nu_s, \nu'_s)$	(PH2 \circ X)
$\Gamma_{\mu\nu i_1 i_2}^{s, \alpha'_1 \alpha'_2} \alpha_1 \alpha_2(s, \nu_s, \nu'_s) = -\xi(\nu) \Gamma_{\mu\nu i_1 i_2}^{u, \alpha_1 \alpha_2} \alpha_1 \alpha'_2(s, \nu_s, -\nu'_s)$	(PH2)
$\Gamma_{\mu\nu i_1 i_2}^{s, \alpha'_1 \alpha'_2} \alpha_1 \alpha_2(s, \nu_s, \nu'_s) = \zeta(\boldsymbol{\alpha})[\Gamma_{\nu\mu i_2 i_1}^{s, \alpha_2 \alpha_1} \alpha'_2 \alpha'_1(s, \nu'_s, \nu_s)]^*$	(X \circ CC)
$\Gamma_{\mu\nu i_1 i_2}^{t, \alpha'_1 \alpha'_2} \alpha_1 \alpha_2(t, \nu_t, \nu'_t) = \zeta(\boldsymbol{\alpha})[\Gamma_{\mu\nu i_2 i_1}^{t, \alpha_1 \alpha_2} \alpha'_1 \alpha'_2(-t, \nu_t, \nu'_t)]^*$	(CC)
$\Gamma_{\mu\nu i_1 i_2}^{t, \alpha'_1 \alpha'_2} \alpha_1 \alpha_2(t, \nu_t, \nu'_t) = -\xi(\mu) \Gamma_{\mu\nu i_2 i_1}^{t, \alpha_1 \alpha'_2} \alpha'_1 \alpha_2(t, -\nu_t, \nu'_t)$	(PH1)
$\Gamma_{\mu\nu i_1 i_2}^{t, \alpha'_1 \alpha'_2} \alpha_1 \alpha_2(t, \nu_t, \nu'_t) = -\xi(\nu) \Gamma_{\mu\nu i_1 i_2}^{t, \alpha'_1 \alpha_2} \alpha_1 \alpha'_2(t, \nu_t, -\nu'_t)$	(PH2)
$\Gamma_{\mu\nu i_1 i_2}^{t, \alpha'_1 \alpha'_2} \alpha_1 \alpha_2(t, \nu_t, \nu'_t) = \zeta(\boldsymbol{\alpha})[\Gamma_{\nu\mu i_2 i_1}^{t, \alpha_2 \alpha_1} \alpha'_2 \alpha'_1(t, \nu'_t, \nu_t)]^*$	(X \circ CC)
$\Gamma_{\mu\nu i_1 i_2}^{u, \alpha'_1 \alpha'_2} \alpha_1 \alpha_2(u, \nu_u, \nu'_u) = \zeta(\boldsymbol{\alpha})[\Gamma_{\nu\mu i_2 i_1}^{u, \alpha_2 \alpha_1} \alpha'_2 \alpha'_1(-u, \nu_u, \nu'_u)]^*$	(X \circ CC)
$\Gamma_{\mu\nu i_1 i_2}^{u, \alpha'_1 \alpha'_2} \alpha_1 \alpha_2(u, \nu_u, \nu'_u) = -\xi(\mu) \Gamma_{\nu\mu i_2 i_1}^{s, \alpha_2 \alpha'_1} \alpha'_2 \alpha_1(u, -\nu_u, \nu'_u)$	(X \circ PH2)
$\Gamma_{\mu\nu i_1 i_2}^{u, \alpha'_1 \alpha'_2} \alpha_1 \alpha_2(u, \nu_u, \nu'_u) = -\xi(\nu) \Gamma_{\mu\nu i_1 i_2}^{s, \alpha_1 \alpha_2} \alpha_1 \alpha'_2(u, \nu_u, -\nu'_u)$	(PH2)
$\Gamma_{\mu\nu i_1 i_2}^{u, \alpha'_1 \alpha'_2} \alpha_1 \alpha_2(u, \nu_u, \nu'_u) = \zeta(\boldsymbol{\alpha})[\Gamma_{\mu\nu i_2 i_1}^{u, \alpha_1 \alpha_2} \alpha'_1 \alpha'_2(u, \nu'_u, \nu_u)]^*$	(CC)

Table II. Symmetry table for the two particle vertices expanded in terms of Pauli matrices [see Eq. (23)] in the asymptotic frequency decomposition. The symmetries are denoted for the s , t and u channel and act as described in the main text.

Appendix E: Susceptibility calculation

We start our calculations from Eq. (46) by inserting Eq. (47) and writing out all necessary quantum numbers. This leads to the following Green's functions

$$G_{\alpha\beta|\alpha'\beta',ij}^{12|11}(t, t'|t, t') = G_{\alpha\beta|\alpha'\beta',ij}^{12|11,c}(t, t'|t, t') + G_{\alpha|\alpha',ii}^{1|1}(t, t)G_{\beta|\beta',jj}^{2|1}(t', t') - G_{\alpha|\beta',ij}^{1|1}(t, t')G_{\beta|\alpha',ji}^{2|1}(t', t) \quad (E1)$$

$$G_{\alpha\beta|\alpha'\beta',ij}^{11|12}(t, t'|t, t') = G_{\alpha\beta|\alpha'\beta',ij}^{11|12,c}(t, t'|t, t') + G_{\alpha|\alpha',ii}^{1|1}(t, t)G_{\beta|\beta',jj}^{2|1}(t', t') - G_{\alpha|\beta',ij}^{1|2}(t, t')G_{\beta|\alpha',ji}^{1|1}(t', t) \quad (E2)$$

$$G_{\alpha\beta|\alpha'\beta',ij}^{22|21}(t, t'|t, t') = G_{\alpha\beta|\alpha'\beta',ij}^{22|21,c}(t, t'|t, t') + G_{\alpha|\alpha',ii}^{2|2}(t, t)G_{\beta|\beta',jj}^{2|1}(t', t') - G_{\alpha|\beta',ij}^{2|1}(t, t')G_{\beta|\alpha',ji}^{2|2}(t', t) \quad (E3)$$

$$G_{\alpha\beta|\alpha'\beta',ij}^{21|22}(t, t'|t, t') = G_{\alpha\beta|\alpha'\beta',ij}^{21|22,c}(t, t'|t, t') + G_{\alpha|\alpha',ii}^{2|2}(t, t)G_{\beta|\beta',jj}^{1|2}(t', t') - G_{\alpha|\beta',ij}^{2|2}(t, t')G_{\beta|\alpha',ji}^{1|2}(t', t) \quad (E4)$$

Since we assume that the Green's functions are diagonal in spin space all terms with $G_{\alpha|\alpha'}$ and $G_{\beta|\beta'}$ vanish. Further we use that for $t \neq t'$ the Green's function $G^{1|1}(t|t')$ vanishes. This assumption breaks for $t = t'$ but since this expression is always inside a Fourier integral and has vanishing weight we

can neglect this edge case. The remaining terms are

$$G_{\alpha\beta|\alpha'\beta',ij}^{12|11}(t, t'|t, t') = G_{\alpha\beta|\alpha'\beta',ij}^{12|11,c}(t, t'|t, t') \quad (E5)$$

$$G_{\alpha\beta|\alpha'\beta',ij}^{11|12}(t, t'|t, t') = G_{\alpha\beta|\alpha'\beta',ij}^{11|12,c}(t, t'|t, t') \quad (E6)$$

$$G_{\alpha\beta|\alpha'\beta',ij}^{22|21}(t, t'|t, t') = G_{\alpha\beta|\alpha'\beta',ij}^{22|21,c}(t, t'|t, t') - G_{\alpha|\beta',ij}^{2|1}(t, t')G_{\beta|\alpha',ji}^{2|2}(t', t) \quad (E7)$$

$$G_{\alpha\beta|\alpha'\beta',ij}^{21|22}(t, t'|t, t') = G_{\alpha\beta|\alpha'\beta',ij}^{21|22,c}(t, t'|t, t') - G_{\alpha|\beta',ij}^{2|2}(t, t')G_{\beta|\alpha',ji}^{1|2}(t', t) \quad (E8)$$

Since the FRG implementation is formulated in frequency space we have to perform a Fourier transformation according to eqs. (13) and (14). To further decompose the two particle connected Green's function we use the tree expansion [62]

$$G(12|1'2') = - \sum_{33'|44'} G(1|3')G(3|1')\Gamma(3'4'|34)G(2|4')G(4|2') \quad (E9)$$

where one then has to insert the decomposition of the vertex (cf. Eq. (2)) and evaluate the sums over the spin indices. We also dropped the indices c denoting connected Green's functions from this point as all following Green's functions will be single particle functions which cannot be disconnected.

For the Heisenberg case ($\Gamma_{\mu\rho} = \Gamma_s \delta_{\mu\rho}$) we then get

$$\begin{aligned}
\chi_{ij}^{\text{Ret}}(\nu) &= \frac{i}{8\pi} \int d\omega (G^K(\omega)G^{\text{Ret}}(\omega + \nu) + G^{\text{Av}}(\omega)G^K(\omega + \nu)) \delta_{ij} \\
&+ \frac{i}{16\pi^2} \sum_{\alpha_3\alpha_3'\alpha_4\alpha_4'} \int d\omega \int d\omega' \left\{ 2\Gamma_{sij}^{\alpha_3'\alpha_4'\alpha_3\alpha_4}(\omega + \nu, \omega'|\omega, \omega' + \nu) \right. \\
&\quad \left. + \Gamma_{sii}^{\alpha_3'\alpha_4'\alpha_4\alpha_3}(\omega + \nu, \omega'|\omega' + \nu, \omega)\delta_{ij} - \Gamma_{dii}^{\alpha_3'\alpha_4'\alpha_4\alpha_3}(\omega + \nu, \omega'|\omega' + \nu, \omega)\delta_{ij} \right\} \\
&\quad \left\{ G^{1|\alpha_3'}(\omega + \nu)G^{\alpha_3|1}(\omega)G^{2|\alpha_4'}(\omega')G^{\alpha_4|1}(\omega' + \nu) \right. \\
&\quad + G^{1|\alpha_3'}(\omega + \nu)G^{\alpha_3|1}(\omega)G^{1|\alpha_4'}(\omega')G^{\alpha_4|2}(\omega' + \nu) \\
&\quad + G^{2|\alpha_3'}(\omega + \nu)G^{\alpha_3|2}(\omega)G^{2|\alpha_4'}(\omega')G^{\alpha_4|1}(\omega' + \nu) \\
&\quad \left. + G^{2|\alpha_3'}(\omega + \nu)G^{\alpha_3|2}(\omega)G^{1|\alpha_4'}(\omega')G^{\alpha_4|2}(\omega' + \nu) \right\} \tag{E10}
\end{aligned}$$

This means that we have to perform a numerical integral in two dimensions which makes this computation more complicated as opposed to the normal evaluation of the flow equations. Since however, the results of the spin susceptibility are final, the integrals do not need to be as accurate as within the flow, where errors get scaled during the flow. Note that in the large S -limit only the sum term and the propagator term

survive[63] while the other contributions are negligible.

For the second case investigated in the paper, which is the Kitaev model the susceptibility has to be evaluated for each spin component separately due to the lack of an $SU(2)$ symmetry. Calculating the spin sums from the vertex decomposition results in

$$\begin{aligned}
\sum_{\alpha\alpha'\beta\beta'} \sigma_{\alpha'\alpha}^x \sigma_{\beta'\beta}^x \Gamma_{\alpha\beta|\alpha'\beta',ij}^{\alpha_3'\alpha_4'|\alpha_3\alpha_4} &= \left\{ 4\Gamma_{xxij}^{\alpha_3'\alpha_4'\alpha_3\alpha_4}(\omega + \nu, \omega'|\omega, \omega' + \nu) \right. \\
&\quad - 2\Gamma_{xii}^{\alpha_3'\alpha_4'\alpha_4\alpha_3}(\omega + \nu, \omega'|\omega' + \nu, \omega)\delta_{ij} + 2\Gamma_{yyii}^{\alpha_3'\alpha_4'\alpha_4\alpha_3}(\omega + \nu, \omega'|\omega' + \nu, \omega)\delta_{ij} \\
&\quad \left. + 2\Gamma_{zzii}^{\alpha_3'\alpha_4'\alpha_4\alpha_3}(\omega + \nu, \omega'|\omega' + \nu, \omega)\delta_{ij} - 2\Gamma_{dii}^{\alpha_3'\alpha_4'\alpha_4\alpha_3}(\omega + \nu, \omega'|\omega' + \nu, \omega)\delta_{ij} \right\} \\
&\quad \delta(\nu + \nu'). \tag{E11}
\end{aligned}$$

$$\begin{aligned}
\sum_{\alpha\alpha'\beta\beta'} \sigma_{\alpha'\alpha}^y \sigma_{\beta'\beta}^y \Gamma_{\alpha\beta|\alpha'\beta',ij}^{\alpha_3'\alpha_4'|\alpha_3\alpha_4} &= \left\{ 4\Gamma_{yyij}^{\alpha_3'\alpha_4'\alpha_3\alpha_4}(\omega + \nu, \omega'|\omega, \omega' + \nu) \right. \\
&\quad + 2\Gamma_{xii}^{\alpha_3'\alpha_4'\alpha_4\alpha_3}(\omega + \nu, \omega'|\omega' + \nu, \omega)\delta_{ij} - 2\Gamma_{yyii}^{\alpha_3'\alpha_4'\alpha_4\alpha_3}(\omega + \nu, \omega'|\omega' + \nu, \omega)\delta_{ij} \\
&\quad \left. + 2\Gamma_{zzii}^{\alpha_3'\alpha_4'\alpha_4\alpha_3}(\omega + \nu, \omega'|\omega' + \nu, \omega)\delta_{ij} - 2\Gamma_{dii}^{\alpha_3'\alpha_4'\alpha_4\alpha_3}(\omega + \nu, \omega'|\omega' + \nu, \omega)\delta_{ij} \right\} \\
&\quad \delta(\nu + \nu'). \tag{E12}
\end{aligned}$$

$$\begin{aligned}
\sum_{\alpha\alpha'\beta\beta'} \sigma_{\alpha'\alpha}^z \sigma_{\beta'\beta}^z \Gamma_{\alpha\beta|\alpha'\beta',ij}^{\alpha_3'\alpha_4'|\alpha_3\alpha_4} &= \left\{ 4\Gamma_{zzij}^{\alpha_3'\alpha_4'\alpha_3\alpha_4}(\omega + \nu, \omega'|\omega, \omega' + \nu) \right. \\
&\quad + 2\Gamma_{xii}^{\alpha_3'\alpha_4'\alpha_4\alpha_3}(\omega + \nu, \omega'|\omega' + \nu, \omega)\delta_{ij} + 2\Gamma_{yyii}^{\alpha_3'\alpha_4'\alpha_4\alpha_3}(\omega + \nu, \omega'|\omega' + \nu, \omega)\delta_{ij} \\
&\quad \left. - 2\Gamma_{zzii}^{\alpha_3'\alpha_4'\alpha_4\alpha_3}(\omega + \nu, \omega'|\omega' + \nu, \omega)\delta_{ij} - 2\Gamma_{dii}^{\alpha_3'\alpha_4'\alpha_4\alpha_3}(\omega + \nu, \omega'|\omega' + \nu, \omega)\delta_{ij} \right\} \\
&\quad \delta(\nu + \nu'). \tag{E13}
\end{aligned}$$

Appendix F: Susceptibility calculation using the Lehmann representation

In this section we are highlighting the calculation for the exact dimer susceptibilities using the Lehmann representation. For this we start by generally calculating the retarded response. For this we use

$$\chi_{ij}^{\mu\nu,\text{Ret}}(t-t') = \theta(t-t') (\chi_{ij}^{\mu\nu,>}(t-t') - \chi_{ij}^{\mu\nu,<}(t-t')) \quad (\text{F1})$$

The greater component is given by

$$\begin{aligned} \chi_{ij}^{\mu\nu,>}(t,t') &= i \langle S_i^\mu(t) S_j^\nu(t') \rangle \\ &= \frac{i}{Z} \sum_n \langle n | S_i^\mu(t) S_j^\nu(t') e^{-\beta H} | n \rangle \\ &= \frac{i}{Z} \sum_n e^{-\beta E_n} \langle n | e^{iH(t-t')} S_i^\mu e^{-iH(t-t')} S_j^\nu | n \rangle \\ &= \frac{i}{Z} \sum_{nn'} \langle n | S_i^\mu | n' \rangle \langle n' | S_j^\nu | n \rangle e^{-\beta E_n} e^{i(E_n - E_{n'})(t-t')} \end{aligned} \quad (\text{F2})$$

Here we used the Heisenberg picture for the spin operators and inserted an identity operation $\sum |n'\rangle \langle n'|$. Note that we did not need to introduce time ordering since the spin operators are located on different branches, and thus contour ordering already fixes the order. Since this expression is only dependent on the time difference $t-t'$ we can reduce this expression to one time variable t . The lesser susceptibility is calculated analogously and reads

$$\chi_{ij}^{\mu\nu,<}(t) = \frac{i}{Z} \sum_{nn'} \langle n | S_i^\mu | n' \rangle \langle n' | S_j^\nu | n \rangle e^{-\beta E_{n'}} e^{i(E_n - E_{n'})t}. \quad (\text{F3})$$

In this expression we renamed $n \leftrightarrow n'$ to achieve a similar structure. Inserting the expressions into Eq. (F1) yields

$$\chi_{ij}^{\mu\nu,\text{Ret}}(t) = \frac{i}{Z} \theta(t) \sum_{nn'} \langle n | S_j^\nu | n' \rangle \langle n' | S_i^\mu | n \rangle (e^{-\beta E_n} - e^{-\beta E_{n'}}) e^{i(E_{n'} - E_n)t}. \quad (\text{F4})$$

Due to the $\theta(t)$ we cannot perform a Fourier transformation directly but have to introduce a small imaginary shift η to ensure convergence as for the free fermions

$$\begin{aligned} \chi_{ij}^{\mu\nu,\text{Ret}}(\omega) &= \lim_{\eta \rightarrow 0} \frac{i}{Z} \sum_{nn'} (\dots) \left[\frac{e^{i(E_n - E_{n'} + \omega + i\eta)t}}{i(\omega + i\eta + E_n - E_{n'})} \right]_0^\infty \\ &= \frac{-1}{Z} \sum_{nn'} \frac{\langle n | S_i^\mu | n' \rangle \langle n' | S_j^\nu | n \rangle}{\omega + i\eta + E_n - E_{n'}} (e^{-\beta E_n} - e^{-\beta E_{n'}}) \end{aligned} \quad (\text{F5})$$

As for the Hamiltonian we choose the Heisenberg dimer with and without pseudo-fermion representation. The partition functions are already given in the main text. Inserting the Hamiltonian then gives

$$\chi_{00}^R(\omega) = \lim_{\eta \rightarrow 0} \frac{1}{4Z} \left[\frac{-2}{\omega + i\eta} (e^{-\beta \frac{J}{4}} - e^{-\beta \frac{J}{4}}) \right] \quad (\text{F6})$$

$$+ \left(\frac{1}{\omega + i\eta - J} - \frac{1}{\omega + i\eta + J} \right) (e^{-\beta \frac{J}{4}} - e^{\beta \frac{3J}{4}}),$$

$$\chi_{01}^R(\omega) = \lim_{\eta \rightarrow 0} \frac{1}{4Z} \left[\frac{-2}{\omega + i\eta} (e^{-\beta \frac{J}{4}} - e^{-\beta \frac{J}{4}}) \right] \quad (\text{F7})$$

$$+ \left(\frac{1}{\omega + i\eta + J} - \frac{1}{\omega + i\eta - J} \right) (e^{-\beta \frac{J}{4}} - e^{\beta \frac{3J}{4}}).$$

For better understanding we can use

$$\lim_{\eta \rightarrow 0} \frac{1}{\omega + i\eta} \rightarrow \mathcal{P} \left(\frac{1}{x} \right) - i\pi \delta(x) \quad (\text{F8})$$

to see that the susceptibility consists of two peaks with opposite signs at $\omega = J$, which come from the first two terms. The last term is vanishing for all frequencies, as the exponentials cancel each other. However, for $\omega = 0$ one has to treat the susceptibility carefully since we formally get a derivative

$$\lim_{E_{n'} \rightarrow E_n} \lim_{\eta \rightarrow 0} \frac{e^{-\beta E_n} - e^{-\beta E_{n'}}}{i\eta + E_n - E_{n'}}. \quad (\text{F9})$$

Performing this derivative leads to the expressions eqs. (49) in the main text.